IEEE Access
Multidisciplinary | Rapid Review | Open Access Journal

Received December 17, 2020, accepted January 4, 2021, date of publication January 18, 2021, date of current version January 26, 2021.

Digital Object Identifier 10.1109/ACCESS.2021.3052478

INVITED PAPER

Sensing Methodologies in Agriculture for Soil Moisture and Nutrient Monitoring

BHUWAN KASHYAP, (Member, IEEE), AND RATNESH KUMAR, (Fellow, IEEE)
Department of Electrical and Computer engineering (ECpE), Iowa State University, Ames, IA 50010, USA

Corresponding author: Bhuwan Kashyap (bkashyap@iastate.edu)

This work was supported in part by the National Science Foundation under Grant CCF 1331390, Grant ECCS-1509420, Grant PFI-1602089, and Grant CSSI-2004766.

ABSTRACT Development and deployment of sensing technologies is one of the main steps in achieving sustainability in crop production through precision agriculture. Key sensing methodologies developed for monitoring soil moisture and nutrients with recent advances in the sensing devices reported in literature using those techniques are overviewed in this article. The soil moisture determination has been divided into four main sections describing soil moisture measurement metrics and laboratory-based testing, followed by in-situ, remote and proximal sensing techniques. The application, advantages and limitations for each of the mentioned technologies are discussed. The nutrient monitoring methods are reviewed beginning with laboratory-based methods, ion-selective membrane based sensors, bio-sensors, spectroscopy-based methods, and capillary electrophoresis-based systems for inorganic ion detection. Attention has been given to the core principle of detection while reporting recent sensors developed using the mentioned concepts. The latest works reported on the different sensing methodologies point towards the trend of developing low-cost, easy to use, field-deployable or portable sensing systems aimed towards improving technology adoption in crop production leading to efficient site-specific soil and crop management which in turn will bring us closer to reaching sustainability in the practice of agriculture.

INDEX TERMS Agriculture, biosensors, electrochemical, electrophoresis, impedance, moisture, nutrient, remote sensing, reflectometry, sensors.

I. INTRODUCTION

Food, water and energy are the key resources that allows for the existence and expansion of humanity. The global demand of these resources has been monotonically increasing and is expected to remain so. According to the United Nations, the global population is expected to reach 9.8 billion by the year 2050 and 11.2 billion in 2100 [1]. With the impact on environment, onset of global warming, major crop producing countries reaching their fresh water limit, unpredictable variability in climate, reduced land fertility from draught, erosion and poor management, and the ever increasing public expectations for more sustainable practices to reduce use of water and agrochemicals, it has never been more important to achieve efficiency and sustainability in agriculture. United States Department of Agriculture (USDA) defines *Sustainable agriculture as an integrated system of plant and animal production practices having a site-specific application that will over the long term satisfy human food and fiber needs, enhance environmental quality and natural resource base upon which the agriculture economy depends, make the most efficient use of nonrenewable resources and on-farm resources and integrate, where appropriate, natural biological cycles and controls, sustain the economic viability of farm operations, and enhance the quality of life for farmers and society as a whole* [2]. Technologies enabling precision agriculture have emerged as one of the key ways to achieve these goals by measuring, monitoring and responding to site-specific variability in the field.

This article aims to present the current state of the sensing methodologies applied in agriculture for soil moisture and nutrient monitoring. The working principles of key technologies are discussed while advances in sensors developed on those principles in recent years, last decade or so, compared (with key works). Section 1 starts with introduction and the aim of this article, section 2 presents the soil moisture

The associate editor coordinating the review of this manuscript and approving it for publication was Fan Zhang.

sensing methodologies, section 3 focuses on the crop nutrient sensing techniques, section 4 discusses the potential of sensing in agriculture going forward, and section 5 presents conclusion.

II. SOIL MOISTURE SENSING METHODS

Water and agriculture are inherently intertwined, where water is one of the key determinants in crop production, agricultural processes affect the hydrological cycle in terms of evapotranspiration, groundwater recharge and runoffs. Over 70% of the global fresh water resources are used by agriculture [3] and at the same time about 4 billion people across the globe live with water insufficiency [4]. Optimum availability of moisture in soil is essential for various biophysical processes like germination of seeds, plant growth, nutrient cycling as well as sustaining natural biodiversity in soil. The importance of soil moisture also makes it a key variable in agricultural monitoring and prediction software tools like USDA's Root Zone Water Quality Model (RZWQM) [5], [6]. Monitoring soil moisture provides key insights into not only the availability of water to crops, but also soil health and moisture retention which are important indicators of sustainable agroecosystem.

Several soil moisture sensing technologies have been developed with various goals in mind such as precision agriculture, landscape moisture statistic monitoring and long term global soil moisture mapping. Soil moisture sensing techniques range from large scale satellite-based remote sensing methods suitable for regional and global scales (100s of km^2) to precision in-field sensors aimed towards plot and field scale (0.1 m^2 to 10000 m^2) measurements. In this section of the article a review of the soil moisture sensing mechanisms and sensors based on those methods are presented. The soil moisture sensing methodologies have been divided into five subsections:

- Soil moisture metrics and laboratory method,
- In-situ soil moisture sensing methods,
- Remote sensing methods for measuring soil moisture,
- Proximal in-field soil moisture monitoring, and
- Other soil moisture sensing methods.

A. SOIL MOISTURE METRICS AND STANDARD LABORATORY METHOD

Soil is a mixture comprising of minerals, organic matter, living organisms, water and gases. The mineral part of the soil can be divided into three size-based particles, sand (largest), silt and clay (smallest). The proportion of each of these types of particles gives the soil its characteristic texture, often based on which the soil type is defined. Water in soil is present in two main forms: (i) bounded, adsorbed on the soil mineral particles and is unavailable to plants. (ii) unbounded, free existing water molecules which are available for absorption by roots, measured in the form of soil water tension/water potential. Depending on the type of soil, the ratio of the water present in bounded and unbounded form varies, for example, clay has particularly high affinity for water molecules, hence soils with larger clay proportions have higher water tensions (more bounded water). Soil moisture sensors can detect either total soil moisture content (SMC) or soil water tension/potential (SWP).

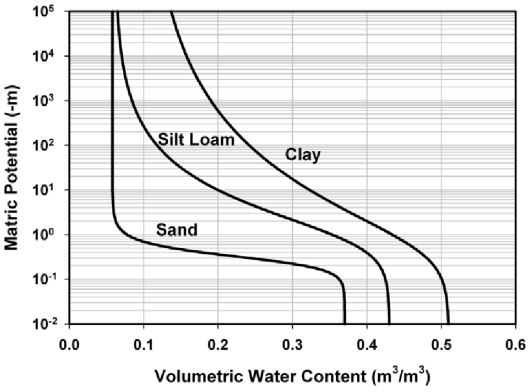

FIGURE 1. Typical soil water characteristic curves for different soil textures, reprinted from [7] with permission from Elsevier.

The relationship between the SMC and SWP is described by the soil water characteristic curve which provides the amount water retained in a soil (SMC) under equilibrium at a given matric potential. The is highly nonlinear and is strongly affected by factors like soil texture, structure and organic matter. Typical soil water characteristic curves for three different soil textures is shown in Figure 1.

SMC is generally expressed on either gravimetric or volumetric basis and can be described as gravimetric water content (GWC) or volumetric water content (VWC), respectively, and are given by,

$$GWC = \frac{m_{wet} - m_{dry}}{m_{dry}} \quad and$$
$$VWC = GWC \times \frac{\rho_{soil}}{\rho_{water}}, \tag{1}$$

where m_{wet} is the mass of the wet soil sample (fresh soil sample), m_{dry} is the mass of the dried soil sample, ρ_{soil} is the dry bulk density of the soil, and ρ_{water} is the density of water, usually taken to be 1000 kg/m^3.

The method most commonly used for determining SMC in laboratories is the thermo-gravimetric method, where the fresh soil sample of known volume is weighed, then oven dried at 105 °C for 24 h and re-weighed, and the difference between the weights provide the amount of the water present in the soil sample [8]. The measured SMC can be expressed in both volummetric and gravimetric units using (1). This technique is highly accurate and simple but, time and labor intensive.

Apart from direct soil water determination in laboratories, several indirect methods have also been developed that are based on the contrasting behaviour of water in terms of its thermal properties like high specific heat capacity, thermal conductivity, and dielectric properties like large dielectric constant as compared to dry soil. Most soil sensors take advantage of these properties to characterize the amount of

TABLE 1. Comparison of some the recent and commonly used *in-situ* point-based soil moisture sensing methods.

Sensor type [Ref.], year	Brief description	Accuracy/ Performance	Range	Strengths	challenges
Tensiometer [9], commercial	Measures SWP using a pressure difference between reference and surrounding	accuracy within 3% of full scale	0 – 100 kPa (SMP*)	Independent of soil type, not affected by electrical conductivity or soil temperature	Requires frequent maintenance, not suitable under freezing conditions, expensive with electronic recorder
Gypsum block or granular matrix sensors [10], commercial	Measures SWP using resistance change of a porous substance in soil	accuracy within 10% to 25% of actual value	0 – 200 kPa (SMP*)	Easy to use, relatively low maintenance, inexpensive (sensor only)	Low accuracy. Salinity and temperature may affect performance, regular maintenance required
Single-probe heat pulse soil moisture sensor [11], 2013	Measures soil water content using heat dissipation properties in soil media.	sensitivity of 0.21 °C per 1% change in VWC	5% to 35% VWC	Low-cost, Independent of soil type and salinity	Energy intensive, ambient temperature and humidity corrections required for good accuracy
Dual-probe heat pulse soil moisture sensor [12], 2017	Measures soil water content using heat dissipation properties in soil media	accuracy within 10%, and sensitivity of actual value	5% to 50% VWC	Relatively low-cost, open-source software and hardware, independent electrical conductivity of soil	Energy intensive, slow response, moderate accuracy
Multi-probe heat pulse SMC sensor [13], 2019	SMC sensor implemented on a compact printed circuit board platform	sensitivity of 0.632 °C per 1% change in VWC	5% to 41% VWC	Relatively low-cost, compact design, uses low energy heat-pulse, independent of soil salinity	Slow response, moderate accuracy, power consumption
Neutron probe sensor [14], commercial	Measures SMC using elastic neutron scattering with hydrogen atoms in soil	within 1% to 5% actual value	0% to 50% VWC	Accurate and fast	Labor intensive (expert operator needed), expensive and cannot be left buried in the soil (radiation hazard)
Time-domain reflectometry-based SMC sensor [15], 2012	Measures SMC from soil dielectric properties calculated using signal propagation velocity along a probe	within 2% (with respect to lab based thermo-gravimetric method)	-	Easy to use, accurate, can measure soil bulk conductivity as well	Expensive, requires soil specific calibration and temperature corrections
Time-domain reflectometry-based SMC sensor [16], commercial	Measures SMC from time interval between signal reflections propagating inside a buried probe	within 2%	0 – 100% VWC	Easy to use, accurate, continuous monitoring	Very expensive
Impedance-based sensor [17]	Multi-frequency impedance measurement using reflection coefficient	within 10 – 15%	0 – 50% VWC	wireless operation, low-cost, ideal for in-situ continuous measurements	Requires soil-type specific calibration, moderate accuracy
Capacitance-based moisture sensors [18]	Measures SMC using capacitance estimation of a probe	within 5 – 10%	3 – 35% VWC	low-cost, capable of measuring SMC at three different depths	Complex calibration
Impedance-based sensor, Decagon EC-5 Moisture [19], commercial	Measures SMC using dielectric properties calculated via impedance measurement of probe buried in soil	within 5%	0 – 60% VWC	Easy to use, continuous measurements, fast response	Requires soil-type specific calibration, and expensive with data logger

*SMP = Soil matric potential; 0 kPa = wet

water in soil for in-field, or proximal, or remote sensing applications.

B. IN-SITU OR AT-SITE SOIL MOISTURE SENSING METHODS

In-situ or at-site soil moisture sensing methods refers to non-destructive *point-based* measurement approaches where the instrument is taken in the field and is in contact with the soil medium. These methods have unique potential to provide real time point-based high resolution moisture content data that is representative of plot to field scale areas and are particularly useful for agricultural applications as they are easier to calibrate, control time scale, can provide measurements at variable depths and in general, more accessible to farmers. Table 1 presents a brief comparison between different in-situ or at-site sensing methods discussed in this article.

1) TENSIOMETER

A tensiometer is a device that mimics the operation of a plant's root, measuring the ease with which a plant can absorb water up from the soil. It consists of a stem filled with distilled water, a porous ceramic tip at the bottom and a pressure/vacuum gauge on the top. It works by releasing or sucking water, to or from the soil through the ceramic tip depending on the water potential difference between the soil mixture and the stem. In dry soil conditions, the water inside the instrument tries to seep into nearby soil creating measurable tension (measured in kPa or centibar). The tension is recorded via a pressure gauge or a transducer that measures pressure. A tensiometer directly measures the water available to the plants (unbounded water content) or the SWP, as opposed to other methods that use indirect soil properties like thermal or electrical, hence it is a highly accurate and a

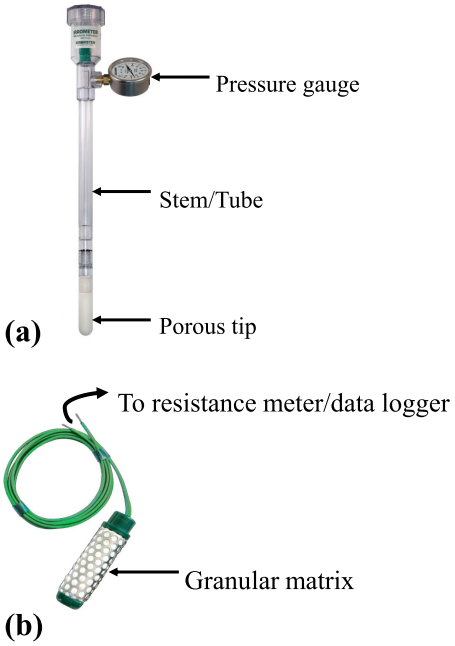

FIGURE 2. (a) Irrometer - a commercial tensiometer. (b) Watermark - a granular matrix SWP sensor. (The Irrometer Co., Riverside, CA; www.irrometer.com).

better indicator of water availability for plants than volumetric or gravimetric water content observations.

Figure 2(a) shows a commercial tensiometer (Irrometer Co., Riverside, CA.) with its main components. Tensiometers have various advantages such as they are not affected by soil temperature or salinity, as the dissolved salts can freely move in and out through the ceramic head and they do not require site-specific calibration based on the type of soil. Tensiometers provides accuracy of up to $\pm 3\%$ of the full scale measurement [9], costing between \$100 to \$300 (not including the electronics or data loggers) [20]. Some disadvantages associated with the device includes frequent maintenance, as the distilled water in the stem needs to be refilled every 2 to 4 weeks depending on the soil type and irrigation frequency, the device has to be removed during winter as freezing temperatures may harm the instrument, and extra care must be taken during deployment as any air pocket around the ceramic head will affect the accuracy of the measurement. Tensiometers and granular matrix sensors are among the most commonly used soil water sensors developed for commercial applications.

2) GYPSUM BLOCK/GRANULAR MATRIX SENSOR

This sensing approach employs a porous material like a gypsum ($CaSO_4.2H_2O$) block or a granular matrix, consisting of gypsum wafers surrounded by porous granular filler material, with electrodes embedded inside. The sensor is buried in soil in the root zone and works on the principle of resistance change depending on the water penetration inside the material. Figure 2(b) shows a commercial granular matrix sensor called Watermark [21]. Gypsum has reasonable solubility in water and begins to dissolve as the moisture from the soil seeps inside the porous matrix/material. This mobilizes the ions inside the porous material reducing the resistance between the electrodes and vice versa. This type of sensor is easy to manufacture, low-priced, and is one of the most prevalent type of sensor used in the field. However, there are some limitations to this method like poor accuracy with error ranging between 10% and 25% [10], slow response time, the gypsum tends to dissolve over time, problems in accuracy as the resistance of gypsum is affected by temperature, and the calibration may vary depending on soil type (or salinity) [22].

3) THERMAL PROBE/HEAT PULSE METHOD

Thermal soil moisture sensing probes measures the temperature of a porous block buried in soil (often made of gypsum or ceramic) or the soil itself, before and after a small heat pulse is applied. The amount of heat dissipation is proportional to the thermal conductivity of the porous block or the soil, which in turn depends on the moisture content in soil. The main components of the sensor include a heating element (like a thermister) and temperature sensor (such as a pn junction), which are embedded in the porous block (gypsum or ceramic) and buried into the soil, measuring SWP or directly buried in soil, measuring SMC. Several thermal probe/heat pulse sensors have been described in literature with single, dual and multi probe designs [11]–[13], [23], [24]. A single-probe heat pulse (SPHP) soil moisture sensor based on a single npn bipolar junction transistor (BJT) was reported in [11], where the collector-base (CB) junction functioned as the heating element and the base-emitter (BE) junction served as the temperature sensor. A generalized relationship between the measured temperature change (ΔT), the heat pulse duration (Δt) and the thermal conductivity of the soil medium (κ) for a single probe heat pulse (SPHP) is given by [11],

$$\Delta T = \frac{-q}{4\pi\kappa} ln(\Delta t), \tag{2}$$

where q is the input heating power per unit length. Either the measured ΔT or the derived κ can be calibrated a function of the moisture in soil. The developed sensor exhibits good sensitivity with respect to the changes in soil water content where 1% change in the water content (VWC) will result in a temperature variation ΔT of 0.21 °C.

Dual probe heat pulse (DPHP) techniques involve separate heater and temperature sensing elements, one such sensor was described for SMC estimation where the heater probe was an insulated copper wire that is folded length-wise to pack into a short steel tube with a K-type or T-type thermocouple for the temperature probe [24]. The DPHP sensor was able to measure SMC between 0 to 30% VWC. Figure 3 shows a general schematic of a DPHP thermal SMC sensor, where the relationship between change in temperature and the radial distance (r) as a function of time (t) and soil thermal

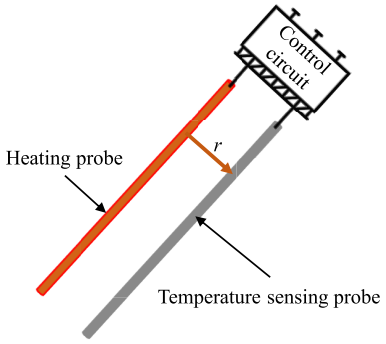

FIGURE 3. General schematic of a dual probe heat pulse soil moisture sensor. 'r' is the radial distance between the probes.

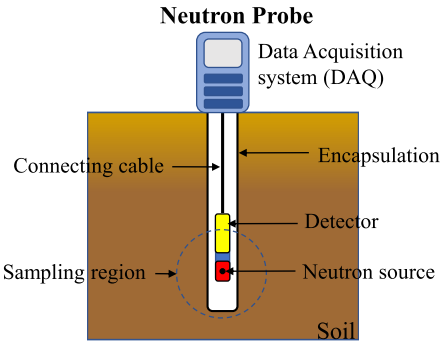

FIGURE 4. Schematic of a neutron probe SMC sensor deployed in the field.

diffusivity (α) can be given by [23],

$$\frac{dT(r,t)}{dt} = \frac{q}{4\pi\kappa t}\, exp(\frac{-r^2}{4\alpha t}). \tag{3}$$

Alternatively, a multi-probe heat pulse sensor has also been reported where multiple temperature sensors are placed around the heater probe, and everything was fabricated on planar PCB platform, where the sensor was able to measure VWC from 5% to 41% with sensitivity of 0.632 °C per 1% change in VWC [13]. Thermal soil water sensors are also commercially available [25] and offer a relatively low-cost solution with accuracy between 5% to 10% [12], but require soil-type specific calibration, show variations in accuracy due ambient temperature and humidity changes, show slow response, and are energy intensive.

4) NEUTRON PROBE METHOD

The neutron probe (NP) method for SMC determination uses the characteristic property of hydrogen nuclei in water molecules to scatter and/or slow down neutrons. Based on the energy transfer, scatter cross-section and having the similar size as a neutron, hydrogen nucleus has greater thermalization (collision) effect with neutrons than any other element. High energy neutrons from a radioactive source, such as radium-beryllium or americium-beryllium slow down or change direction due to elastic collisions [26]. The thermalized neutron density can easily be measured by a detector and if the capture cross-section of soil media remains fairly constant i.e. the chemical composition remains fairly constant except the variation due to water, the measurements from neutron probes can be calibrated to represent the SMC.

Figure 4 shows the schematic of a neutron probe soil moisture sensor where the general construction of the device consists of a radioactive neutron source and a detector connected through a cable. The high energy neutrons are released by the radioactive source that collide with hydrogen atom nuclei of water in soil and are captured by the detector. Neutron probes are available commercially where, with good calibration based on soil make up (metal content and density) and proper installation (sampling region completely buried in soil and minimal air gaps around the probe), precision between 1% to 5% can be achieved [14]. Some advantages of NPs include high accuracy, and relatively less dependence on soil temperature and salinity. Some limitations of this method include radiation hazard, the requirement of a skilled operator to properly install and take measurements making the method labor as well as cost intensive.

5) TIME DOMAIN REFLECTOMETRY-BASED METHOD

The time domain reflectometry (TDR) is a well known technique that was originally developed for detecting faults across transmission lines by observing the reflections from impedance mismatches and the time interval based on the velocity of the electromagnetic (EM) signal along the transmission line [27]. TDR-based SMC measurement works by determining the propagation velocity of EM signal in the soil and using it to calculate the permittivity/dielectric constant. Soil can be considered as a mixture of water, dry soil/matter and air, where water has a specifically high dielectric permittivity, $\varepsilon_{water} = 80$ at room temperature as compared to air, $\varepsilon_{air} = 1$ and dry soil/matter, $\varepsilon_{drysoil} =$ 3-5, hence, the overall permittivity of the soil is highly dependent on its water content.

TDR-based SMC sensors consist of a transmission line made of parallel metallic probes of length L completely buried in soil at the required depth. As the signal propagates, a part of an incident EM wave is reflected at the interface where the cable connects to the probe because of the impedance mismatch as the cable and the probe may have different characteristic impedance, the rest of the wave propagates through the probe to the tip buried in soil and is reflected back. The propagation velocity v along the TDR probe buried in soil is given from [28] as:

$$v = \frac{1}{\sqrt{(\mu_s\varepsilon_s/2)(\sqrt{1+\tan^2\delta}+1)}}, \text{ with} \tag{4}$$

$$\varepsilon_s = (\varepsilon_s' - j\varepsilon_s'')\varepsilon_0 = \varepsilon_s'\varepsilon_0 - j\frac{\sigma_s}{\omega};$$

$$\tan\delta = \frac{\text{Imaginary}(\varepsilon_s)}{\text{Real}(\varepsilon_s)} = \frac{\sigma_s}{\omega\varepsilon_s'\varepsilon_0},$$

where ε_s is the complex permittivity of soil, $\varepsilon_0 = 8.854 \times 10^{12}$ (F/m) is the permittivity of the free space, ε_s' and ε_s'' are

the real and imaginary parts of relative permittivity, respectively, of soil, $\tan\delta$ is the loss tangent, σ_s is the electrical conductivity of soil, μ_s is the permeability of soil, and ω is the angular frequency of measurement. Soil in general has relatively low electrical conductivity (small σ_s) and at signal frequencies of the order of 1 GHz or higher (large ω), ε_s'' and $\tan\delta$ are small. Using these approximations, the propagation velocity v of the EM wave in soil can be expressed from (4) as:

$$v \approx \frac{1}{\sqrt{\mu_s \varepsilon_s}} \approx \frac{c}{\sqrt{\varepsilon_s'}}, \tag{5}$$

where $c = 1/\sqrt{\mu_0 \varepsilon_0}$ and $\mu_0 = 4\pi \times 10^{-7}[V.s/(A.m)]$ are the speed of light in free space and the magnetic permeability, respectively. Given the length of the probe and the measured time interval between reflections t, the measured propagation velocity of the EM signal in soil can be expressed as:

$$v = \frac{2L}{t}. \tag{6}$$

From (5) and (6), the dielectric permittivity of soil can be calculated as:

$$\varepsilon_s' = \left(\frac{ct}{2L}\right)^2. \tag{7}$$

The dielectric constant of the soil obtained from (7) is used to relate to the VWC, denoted θ_v, through a calibration function that can be described as $\theta_v = f(\varepsilon_s')$. Various models for the calibration function f have been discussed in literature. One such well-known empirical calibration function was presented in [28] and has the form:

$$\theta_v = -5.3 \times 10^{-7} + 2.92 \times 10^{-2}\varepsilon_s' - 5.5 \times 10^{-4}\varepsilon_s'^2 + 4.3 \times 10^{-6}\varepsilon_s'^3. \tag{8}$$

(8) was shown in [28] to hold universally for most mineral soils with minimal dependence on soil temperature, salinity, and texture. However, many other works have been reported on the calibration function estimation based on soil type [29], [30], temperature corrections [15] and effect of temperature on TDR-based soil permittivity estimation depending on the proportions of bound and free water in soil [31], and dielectric mixing models that expands the water in the soil mixture to free water and bound water bringing the number of phases to four, dry soil and air being the other two [32]. Overall, the TDR method for SMC determination has high accuracy of within 2% with respect to the standard thermogravimetric laboratory-based method and can also be used to measure bulk conductivity of soil [15]. The stimulus EM signal used is a rectangular pulse waveform with frequency of the order of 1 GHz and the time resolution for the reflection intervals of the pulses is in the range of 10 ps [15]. Hence, sophisticated data analysis methods as well as circuits are required to record the reflection times accurately making the probes expensive.

TDR soil sensors are also readily commercially available offering accuracy in VWC within ±2% can cost between $1500 to $7500 (including data reader) making it an expensive sensing method [16], [33].

FIGURE 5. A commercial TDR moisture meter: HandiTrase TDR Soilmoisture Meter w/FLD Probe [16].

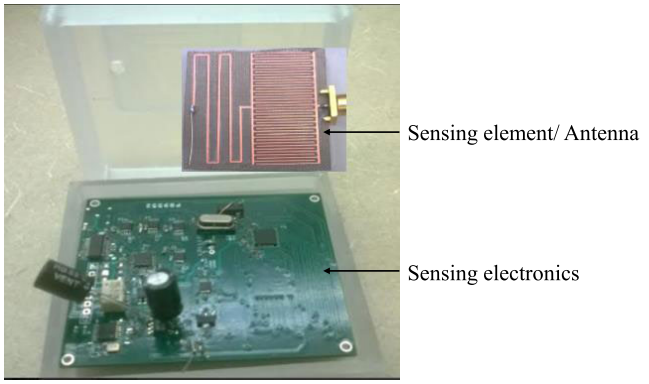

FIGURE 6. An impedance spectroscopy-based in-situ soil moisture sensor with the sensing element also serving as an antenna ©[2018], IEEE [36].

6) IMPEDANCE/CAPACITANCE-BASED METHODS

Impedance/capacitance-based SMC measurement methods rely on the effect of moisture content on the overall dielectric permittivity of soil, similar to TDR-based SMC sensors. Where TDR sensors use the time delay measurement to determine the permittivity of soil, the impedance/capacitance sensors measures the impedance or the capacitance of a buried probe or planar structure which depends directly on the permittivity of the soil. These sensors operate in comparatively lower frequency ranges (10s of MHz) which makes the application specific circuit design simpler than the TDR-based method. There are two main component of an impedance-based SMC sensor, (i) the sensing element or the probe, and (ii) the impedance or capacitance measurement circuit. Numerous strategies involving single as well as multi frequency impedance measurements have been explored in literature [18], [27], [34], [35]. Some of the key recent sensing systems built in the past decade for in-field determination of the SMC are discussed here.

A low RF band impedance spectroscopy-based sensor for in-situ, wireless soil sensing was developed in [17], [37]. The system uses a planar microstrip electrode as the sensing element in contact with the soil which also doubles as the antenna for wireless communication, operating at 433 Mhz. Impedance measurement circuit was fabricated on a printed circuit board (PCB) and was capable of measuring the

reflection coefficient (Γ_{soil}) from the incident and the reflected signals at multiple frequencies ranging between 3 MHz to 30 MHz. The impedance of the sensing element was then calculated according to the following equation,

$$\Gamma_{soil} = \frac{V_r}{V_i} = \frac{Z_{soil} - Z_0}{Z_{soil} + Z_0}, \tag{9}$$

where V_r is the measured reflected signal, V_i is the measured incident signal, Z_{soil} is the calculated soil impedance and Z_0 is the characteristic impedance of the transmission line connected to the sensing electrode (typically, 50 Ω). (9) provided the complex impedance whose real and imaginary parts indicated the conductivity and the SMC, respectively. The sensing system showed accuracy within 10% of true value, and was designed to be left buried underground for continuous SMC measurements. In a later extension of the work, dielectric mixing models were explored using the impedance measurement data to estimate salinity along with SMC [36].

A miniaturized wireless water content and conductivity soil sensor system was developed recently, where impedance measurements were taken at a low (100 kHz) and a high frequency (10 MHz) points which described the resistance and the capacitance of the soil between the electrodes, respectively. An excitation signal of known amplitude is applied, then the signal amplitudes at the electrodes are determined by a peak detector. The peak detector creates a DC signal proportional (theoretically) to the amplitude of the AC response of the soil electrodes [38].

A low-cost soil moisture profile probe using thin-film capacitors and a capacitive touch sensor is presented in [18]. Thin film rectangular electrodes were fabricated by etching copper (Cu) on polyethylene terephthalate (PET) film. The film was then rolled onto a polyvinyl chloride (PVC) pipe where a distance of 1 mm was kept between the rectangular Cu electrodes forming a capacitor and a set of three electrodes were made at depths of 10 cm, 20 cm and 30 cm. Temperature sensors using thermistors were also placed adjacent to the electrodes. The sensing electronics consisted of a low cost capacitive touch sensor controller MPR121 (NXP Semiconductors N.V., Eindhoven, The Netherlands) to measure capacitance through the constant current source method at a frequency of 62 kHz. The method works by driving a constant current I into the capacitor for a unit time period t, and measuring the voltage V across the capacitor C as:

$$V = \frac{I \times t}{C}. \tag{10}$$

Based on the sampled data, a linear, a quadratic and a cubic empirical calibration functions were derived for VWC at the depths of 10 cm, 20 cm, and 30 cm, respectively. The calibration function showed good coefficient of determination (R^2) values between 0.91 and 0.95 with accuracy within 5% of true value. The overall sensing system was estimated to cost around $200-$300.

In another work, the design and calibration of a low cost capacitive SMC sensor with flexible connection to dataloggers via an analog output and an SDI-12 communication protocol was pursued [35]. The system allowed flexibility in choosing pre-registered calibration functions depending on soil type, where equations were made available for three different soil types. The sensing electronics consisted of an oscillator employing integrated circuit (IC) 555 in an astable configuration that generates a square wave whose frequency varies with the capacitance of the probe. A picoPower 8-bit AVR RISC-based microcontroller from Microchip (Chandler, AZ, USA) was used for processing and control. Two parallel copper tracks on a PCB formed the sensing probe. The sensing circuits as well as the sensing probe were integrated together on a single compact PCB substrate as shown in figure 7. The sensor was calibrated against the data from a commercial sensor, MPS-6 (Decagon Devices, Inc.) in the field for 1 month where the data was remotely recorded using a CR1000 datalogger every 10 mins. The sensor accuracy was shown to be within ±7% VWC.

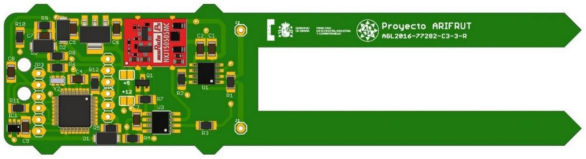

FIGURE 7. Experimental Sensor design on a PCB developed in [35].

Overall, the impedance-based methods provide opportunities for developing low-cost, field-deployable SMC sensors with a few drawbacks such as soil-type specific calibration and need for temperature corrections to achieve high accuracy [35]. Impedance or capacitance-based probes are also commercially available detecting both soil water potential [39] and SMC within 2%-5% accuracy [19].

C. REMOTE SENSING METHODS FOR SOIL MOISTURE ESTIMATION

Several satellite-based remote sensing systems for soil moisture monitoring have been reported in literature [40], [41]. In 2015, NASA launched its first Earth satellite designed to collect global observations of the vital soil moisture called the Soil Moisture Active Passive (SMAP) satellite [42], [43]. Remote sensing (RS) methods for SMC (RS-SMC) determination are particularly suitable for regional to global scale measurements and are based on either reflected or emitted electromagnetic (EM) energy from the soil surface. The methods can be broadly classified into two main categories: (i) Active methods where the reflected or scattered energy is recorded in response to incident energy, and (ii) Passive methods where sensors (like radiometers) are used to detect the radiation emitted by the target also known as the brightness or the brightness temperature of the target. Techniques have been developed for observing SMC remotely in the following EM spectral ranges: visible, infrared/thermal and microwave, where the soil moisture is determined based on the intensity variations of the radiation due to parameters like dielectric constant, temperature, and thermal properties. Secondary parameters such as vegetation cover, surface

roughness and atmospheric effects also play an important role in successful RS-SMC retrieval. Vast amounts of RS-SMC data from various satellite missions has been observed and processes in literature [44], [45], a brief review of the key methods in RS-SMC estimation are presented here.

Optical methods using reflectance spectroscopy were among the early techniques applied for RS-SMC observations operating in the visible (vis) or near-infrared (IR) region of the EM spectrum. Majority of the sun's radiation directly reflected from the earth's surface lies in the 0.4-2.5 μm wavelength range within which water molecules exhibit distinct absorption bands [46], and reflectance spectroscopy exploits this characteristic property of the water molecules to quantify skin SMC. An early work on spectrophotometric determination of soil water content based on the absorbance of water at 1.94 μm wavelength was presented in [47], and a linear response between the absorbance amplitude and SMC was observed. Since then, numerous works have been reported on reflectance based method in vis, near-IR, and short-wave-IR spectral ranges for RS-SMC determination [45], [46]. Although surface reflectance-based methods in the visible-infrared range have the potential to provide relatively higher spatial resolution data, it is limited to skin RS-SMC measurements, and the spectral behavior of soil surface is influenced not only by SMC but also by other parameters such as surface roughness, soil type, vegetation, topography and atmospheric conditions.

Moving to higher wavelengths, in the *thermal-IR* region between 3.5 μm-14 μm, SMC can be retrieved using thermal properties of soil. Water has distinctly high specific heat capacity, hence, the overall soil thermal inertia (P) is highly influenced by the SMC and can be expressed as,

$$P = \sqrt{\lambda_s \rho_{soil} C_{soil}}, \tag{11}$$

where λ_s is the thermal conductivity of soil, ρ_{soil} is the soil bulk density, and C_{soil} is the soil heat capacity. When the moisture content in soil increases, the thermal inertia also increases which reduces the diurnal amplitude variations in the land surface temperature (LST). A generalised inverse linear relationship between SMC and LST can be given by,

$$SMC = \frac{LST_{dry} - LST}{LST_{dry} - LST_{wet}}, \tag{12}$$

where LST_{dry} and LST_{wet} are the known LSTs for dry and wet soil conditions, respectively. SMC obtained from (12) is also known as the Normalized Difference Temperature Index (NDTI). A list of satellites with LST capable sensors is reported in [48], and various indices, including NDTI, for SMC quantification have been summarized in [46]. LST-based measurements are restricted to soil surface temperatures and face interference from vegetation covers.

Approaches combining *both optical and thermal* methods to determine RS-SMC using LST and vegetative index (VI), which is results from the reflectivity of vegetation other objects in any particular frequency band, have also been developed. In the past three decades, LST-VI-based methods have been extensively applied towards SMC determination [45], [46], [49]. The estimation of moisture in a soil-vegetation/LST-VI system is based on the energy balance equation:

$$R_n = H + LE + G, \tag{13}$$

where R_n is the net radiation, H is the sensible heat flux (heat energy exchange responsible for change in temperature), LE is the latent heat flux (evapotranspiration), and G is the soil heat flux. Therefore, SMC in the root zone can be indirectly estimated over vegetated area through the thermal response of the vegetation canopy. Different formulations based on the energy balance equation as well as various LST-VI indices to quantify SMC, evapotranspiration, leaf area index, and more from remote sensing data have been developed in the past [49]–[51]. The trapezoid or triangle model is one of the most commonly applied approaches where SMC can be estimated from the pixel distribution in the LST-VI feature space [45], [49].

RS-SMC estimation in the *microwave* wavelengths, $1\ mm - 30\ cm$, have been observed to be more robust than vis-thermal methods, as microwaves are better suited for passing through clouds and penetrating deeper under the soil surface as well as through vegetation (especially at lower frequencies) but provide limited spatial resolution. *Passive microwave sensors (radiometers)* measure the radiation naturally emitted by the soil surface in the form of its brightness temperature (T_B), moist soils appear cooler to radiometers. The intensity of the observed emission is proportional to the product of the temperature (T_{surf}) and emissivity (e) of soil [40], and the recorded T_B by the radiometer, and can be given as:

$$T_B = \tau(rT_{sky} - eT_{surf}) + T_{atm}, \tag{14}$$

where τ is the atmospheric transmission, rT_{sky} is the reflected sky brightness temperature (r is the surface reflectivity), and T_{atm} is the temperature contribution of the atmosphere. Multiple algorithms have been developed for SMC retrieval using T_B, summarized in [52]. The modeling generally consist of two main steps: (i) Radiative transfer model, relating T_B and soil dielectric constant (ε_s), and (ii) Dielectric mixing model for relating SMC (VWC) with ε_s.

Active microwave sensors (radars) record the backscattered signal when a beam of microwave radiation is incident on the ground. The microwave backscatter is dependent on the soil variables like moisture, vegetation cover and surface roughness (typically at higher resolutions). Among physical models, integral equation model is commonly used for the backscatter coefficient calculations [52]. Various empirical and semi-empirical models have also been reported along with machine learning-based approaches [52], [53].

Although satellite-based remote sensing for soil moisture content provides appealing solutions for long-term large scale measurements, it has coarse spatial (of the order of km^2) and temporal resolutions and are restricted to shallow penetration

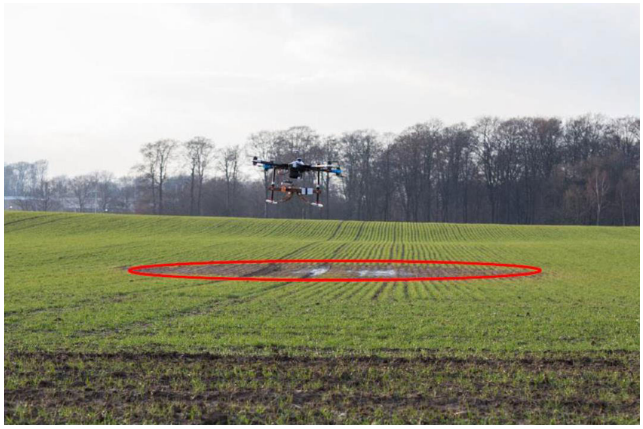

FIGURE 8. A drone-borne GPR-based sensing platform for SMC determination, reprinted from [54] with permission from Elsevier.

depths. They also require complex data analyses which may vary depending on the governing group, making the SMC data accessibility difficult for individual fields and farmers for precise agriculture resource management.

D. PROXIMAL IN-FIELD SOIL MOISTURE MONITORING

Proximal in-field soil moisture sensors refer to devices that are not in direct contact with the soil but are in *proximity* to the soil surface for *non-point*-based estimation. Such sensing systems consist of airborne as well as land-borne techniques for plot and field scale SMC measurements. Ground penetrating radar (GPR) systems mounted on unmanned aerial vehicles (UAVs) or drones have emerged as one such promising proximal SMC determination method. A recently developed system is shown in Figure 8 and presents a drone-borne GPR sensor for soil moisture mapping using a lightweight vector network analyzer (VNA) combined with a hybrid horn-dipole antenna, a lightweight global positioning system (GPS), a computer system and a smartphone [54]. Reflection coefficient or return loss ($S_{11}(\omega)$) is measured using the single port VNA in the 500 MHz to 700 MHz frequency range. $S_{11}(\omega)$ refers to the scattering parameter which is calculated as the ratio of the reflected to the incident power at port 1 in a given system. The frequency was chosen to avoid soil surface roughness effects and sample the SMC between 10 cm to 20 cm soil depth. The data processing was done in two main steps: (i) Radar modeling, where the VNA-antenna-multilayered medium (soil) were modeled as linear systems in series and parallel in the frequency domain, as described in [55], resulting in the overall transfer function as:

$$S_{11}(\omega) = R_i(\omega) + \frac{H_t(\omega)G_{xx}(\omega)H_r(\omega)}{1 - H_f(\omega)G_{xx}(\omega)}, \qquad (15)$$

where $R_i(\omega)$, $H_t(\omega)$, $H_r(\omega)$ and $H_f(\omega)$ are the complex return loss, transmitting, receiving and feedback loss transfer functions, respectively, and $G_{xx}(\omega)$ is the transfer function (Green's function) of the air-subsurface system modeled as a multilayered medium. $R_i(\omega)$ can be calculated by operating the system in free space ($S_{11}(\omega) = R_i(\omega)$), and $H_t(\omega)$, $H_r(\omega)$ and $H_f(\omega)$ were obtained by solving a system of linear equations [55]. Hence using (15), $G_{xx}(\omega)$ was calculated from the measured $S_{11}(\omega)$. (ii) Full-wave inversion for parameter retrieval, namely, an inverse problem was defined using weighted least-squares formulation and the minimization of the following objective function ($\Phi(b)$) was carried out:

$$\Phi(b) = (g^*_{xx}(t) - g_{xx}(b,t))^T (g^*_{xx}(t) - g_{xx}(b,t)), \qquad (16)$$

where $g^*_{xx}(t)$ and $g_{xx}(b,t)$ are the experimental and the modeled Green's function in time domain, $b = [h, \varepsilon_s]$ with h being the vector of the distance between the antenna center and the soil surface and ε_s being the vector of relative dielectric permittivity of soil. The experimental $G_{xx}(\omega)$ calculated from (15) was used to calculate $g^*_{xx}(t)$ using inverse Fourier transform. The VWC was then calculated from the ε_s measurement using TDR equation (8). High-resolution SMC maps were obtained using the developed system in three agricultural fields in Belgium.

UAV-based high resolution thermal and multi-spectral imagery coupled with image processing algorithms have also been applied for proximal SMC determination. These imaging techniques are similar to satellite-based remote sensing methods but provide higher spatial resolutions due to close proximity to surface. In a recent work, *nine* vegetative indices (VIs) related to water stress in maize at different growth stages were derived from UAV multi-spectral imagery and weather conditions, and were used to establish a crop water stress index (CWSI) inversion model, which was then compared with CSWI obtained from on-site ground-based SMC measurements [56]. The ratio of transformed chlorophyll absorption in the reflectance index (TCARI) and renormalized difference vegetation index (RDVI), and the TCARI and soil-adjusted vegetation index (SAVI) had high correlations with CWSI. R^2 values were 0.47 and 0.50 for TCARI/RDVI at the reproductive and maturation stages, respectively; and 0.81 and 0.80 for TCARI/SAVI at the late reproductive and maturation stages, respectively. Overall, the study reported on the feasibility of using UAV-based imagery for SMC detection on field scale with moderate accuracy.

In another work, an artificial neural network (ANN)-based model using a three-layered feed forward neural network was developed with multi-spectral images recorded via *AggieAir* [57] platform, consisting of UAV that can carry multispectral sensor load, as inputs to estimate soil moisture [58]. Normalized Difference Vegetative Index (NDVI), Vegetative Condition Index (VCI), enhanced vegetation index (EVI), RGB, NIR and thermal imagery were used as inputs. Finally, the ANN model with 8 input parameters (red, blue, NIR, thermal, NDVI, VCI, EVI and field capacity) was reported to perform the best with R^2 value of 0.77 with respect to the ground-based SMC measurement. An advantage of data driven (ANN) based approach over conventional SMC estimation using empirical models based on indices like VIs

and LSTs is that, indices-based methods require large number of pixels to be sampled in order to have enough points in an image to use in the determination of the boundaries of extreme conditions. ANN-based modelling has the potential to provide better resolutions and robust results but require more complex computations as well as care must be taken in selecting and processing input parameters and modeling structures.

The key advantages of UAV-based SMC sensors include ability to cover relatively larger areas, autonomous operation, potential to add other sensing technologies like imaging for weed detection and crop scouting, and the demand for drones in agriculture is predicted to increase rapidly [59]. Some limitations include complex data processing is required, accuracy in SMC estimates is lower than in-situ methods, uneven terrain may cause errors, environmental conditions like snow cover and rainfall may affect the measurement, and UAVs can cost of the order of $10000, but can break even after a few uses [59]. There also exist considerations for use of UAVs in form of the rules laid down by the Federal Aviation Administration (FAA), such as the total weight must not exceed 55 pounds, maximum allowable altitude is 400 *ft* above ground, etc. [60].

Electromagnetic induction (EMI)-based methods can also be identified as land-borne proximal SMC sensors. EMI sensors work by measuring apparent electrical conductivity of soil, which positively correlates to the water in soil as more ions gets mobilized with higher SMC, by inductive coupling. The sensing structure is composed of transmitter (Tx) and receiver (Rx) coils, where Tx coils are energized with alternating current (AC) and generate time-varying EM fields that induces circular eddy currents in the nearby conducting media (soil). Weak eddy currents in soil in turn generates secondary EM fields that induces AC current in Rx coils. The amplitude and phase difference between Tx and Rx currents is then used to determine soil properties. EMI-based sensors are better suited to determine SMC in drier soils with higher electrical resistivities. However, the result from the sensors can vary depending on variable soil properties such as salinity and metallic ion content mandating soil-type specific calibration for sufficient accuracy, and generally requires special expertise for operation in the field. Overall, EMI-based soil sensing is a relatively mature technique with numerous commercially available sensors, both handheld as well as vehicle mounted [61].

E. OTHER SOIL MOISTURE SENSING METHODS

In addition to the aforementioned sensing approaches, other relatively uncommon but innovative technologies have been applied towards soil moisture determination primarily on *non-point-based* field to catchment scale and beyond. In one such method, soil moisture sensing using *wireless underground communications* was reported, where the relative permittivity of soil and soil moisture is determined using wave propagation velocity and path loss between an underground transmitter (Tx) and receiver (Rx) [62]. The proposed sensing model was validated through experiments in a software-defined radio test-bed and an indoor test-bed in the frequency range from 100 MHz to 500 MHz using dipole antennas with over-the-air resonant frequency of 433 MHz, where the Tx and Rx were buried in different types of soil at depths of 10 cm, 20 cm, 30 cm and 40 cm. The reported system was capable of measuring soil moisture and permittivity in 1 m to 15 m distance range between Tx and Rx, and exhibited accuracy within 8% estimation error from ground truth. However, for practical implementation such a system may be power intensive as well as come with high initial set-up cost.

Similar to the methodology of neutron probes, *cosmic ray neutron probes* (CRNPs) have also been reported for determining SMC, where instead of employing radioactive neutron emitting components, cosmic ray neutron intensity is recorded near the surface. The elastic collisions with soil water plays a moderating role as the cosmic neutron diffuse through soil and can be calibrated to estimate SMC. CRNPs commonly provide data on intermediate/field scale, and are restricted to shallow depths [63]. Software modelling tools for field scale soil moisture maps using CRNPs have been developed and are being continuously improved [64], [65]. An intermediate scale CRNP-based system called COsmic-ray Soil Moisture Observing System (COSMOS) was described in [66]. The system consists of deploying CRNPs above surface, measuring secondary neutrons, at several locations (about 500 in total) across the United States to measure average SMC within a diameter of a few hectometers and depth of a few decimeters. Another work reported on the extension of cosmic-ray neutron probe measurement depth for improving field scale root-zone soil moisture estimation by coupling with representative in-situ sensors [67]. Overall, similar to NPs, CRNPs can provide highly accurate average SMC measurements on intermediate scale within 2% estimation error depending on the calibration and operating conditions [66].

Global navigation satellite system reflectometry (GNSS-R) or Global positioning system reflectometry (GPS-R) is another relatively new but promising technology applied for SMC estimation at intermediate to large scales [68]. It works by recording GNSS/GPS signal power variations received by an antenna on the ground, directly from the satellite versus through reflected pathways from the surface. The simultaneously received direct and coherently reflected signals results in an interference pattern which produces a modulation that can be observed in temporal variations of the signal-to-noise ratio (SNR) data recorded by the receiver on the ground. All the three GPS interferogram parameters: effective reflector height, phase and amplitude are a function of the soil surface permittivity which in turn depends on the near surface SMC, within the top 5-6 cm of the soil [69]. A GPS multipath-based near surface SMC estimation system was developed in [70], where the sensitivity of the recorded GPS SNR data with respect to moisture variations in the areas of 1000 m^2 horizontally and 1-6 cm vertically was observed. The following

model was described for SNR [70],

$$SNR = A\cos\left(\frac{4\pi h}{\lambda}\sin E + \phi\right), \tag{17}$$

where A is the amplitude, h is the height above the horizontal reflector, λ is the GPS wavelength and E is the elevation angle of the satellite and ϕ is the phase offset. An unweighted least squares fit to the GPS SNR data (restricted to 5–25 degrees elevation angles) was used to find A and ϕ, which were then correlated to SMC using linear and polynomial fits with R^2 between 0.9 and 0.76, when compared with the average SMC measurements taken using in-situ reflectometry-based sensors. Most disagreement was observed when SMC was less than 10% VWC. In another work, phase-only was established as the best metric derived from GPS data to estimate SMC [69].

A long-term GNSS-R-based SMC determination case study for Sutherland, South Africa was reported in [71], where time series GNSS SNR data was recorded and used to estimate soil moisture variations during 2008 to 2014. A model similar to 17 was used to calculate the phase and amplitude from the SNR data which was then correlated with SMC obtained using in-situ TDR-based measurements with reported R^2 of 0.8. The results captured the the wetting and drying cycles in response to rainfall.

It can be concluded that GNSS-R holds potential to provide complementary intermediate scale SMC estimates worldwide using the established GNSS infrastructure.

F. FUTURE PROSPECTS AND RESEARCH DIRECTION IN SOIL MOISTURE SENSING

In order to successfully implement precision site-specific management, accurate soil property maps are essential. For this purpose, continuous progress is being made on small-scale point-based in-situ methods, and large-scale remote sensing technologies, as well as intermediate-scale proximal soil sensing techniques for soil moisture determination. Presently, tensiometer, TDR- and impedance-based sensing probes are among the most readily available and applied for *in-situ* point-based soil moisture monitoring. Currently, the devices based on these methods require continuous maintenance and human intervention in terms of proper installation, feeding power and data collection which restricts their use when obtaining high resolution soil moisture maps of a field or plot. However, the advent of internet-of-things (IoT) and wireless sensing technologies, particularly the ones that can be left buried (up to 1 m or so) in soil for long periods of time (2 to 5 years) such as described in [17], [38], [72], can enable fully automated operation. By placing the sensors underground, measurements can be taken at strategic locations without interrupting on-land activities facilitating accurate site-specific management. In the future, for point-based applications, SMC monitoring technologies not only need to be accurate but also power efficient and economical with easy data access and analysis resulting in functional information for growers.

Alternatively, for obtaining soil moisture maps at intermediate scale, UAV-based proximal sensing methods are promising as they require minimal hardware and human intervention for covering relatively larger land areas. Continuous progress is being made in UAV-imaging, and GPR-based technologies for improving spatial as well as depth resolution of SMC measurement, which currently are inferior to point-based methods. Though expensive at first, with continuous use, proximal/UAV-based sensors can prove to be economical. These methods offer unique advantage in terms of easier adoption, and flexibility in the type of sensors that can be mounted on a UAV with potential to provide supplementary information about soil and plant characteristics like crop health, vegetation cover and more.

On an even larger spatial and/or temporal scale satellite-based remote sensing methods are uniquely suitable. The soil moisture information obtained using these methods can be used for agricultural applications but is more suited for large-scale geological and hydrological studies. These methods are especially useful for observing soil or land characteristics over longer time scales spanning decades over large areas spanning continents. However, the RS-SMC measurements are presently restricted to near-surface (at depths of a few *cm*) observations. Constant progress is being made in improving remote sensing hardware as well as software for realizing higher accuracy as well as resolution in satellite-based soil moisture determination. Data processing and analysis plays a major role in SMC retrieval, making these methods complex, however, the emerging data analysis techniques based on empirical models as well as machine learning methods can provide robust measurements with minimal error due to surface variations such as vegetation cover, roughness, and temperature, and are an active area of research with applications spanning even beyond earth.

III. CROP NUTRIENT SENSING METHODS

For the majority of Earth's history, nutrient cycling had occurred naturally from soil to plants and animals, and then back to soil through decomposition of biomass. As humans went from hunter-gatherers to practicing agriculture and developing long term settlements, the natural soil nutrient cycling was altered through production and application of agrochemicals (chemical fertilizers, pesticides, herbicides, etc.). In the mid 20^{th} century agriculture was further transformed by the green revolution that increased the crop production worldwide through selective breeding for developing and adopting high yielding crop varieties, especially cereal and novel cultivation practices. Ever since then, achieving sustainability through precision agriculture has been a goal for humanity.

In general, it has been established that there are 17 essential elements/nutrients that are critical for plant growth, and deficiency of any one of them can result in reduced yields [73]. Figure 9 presents the essential elements and the form in which they are taken up by the plants. The non-mineral elements, C, H and O are available to the plant either from the atmosphere

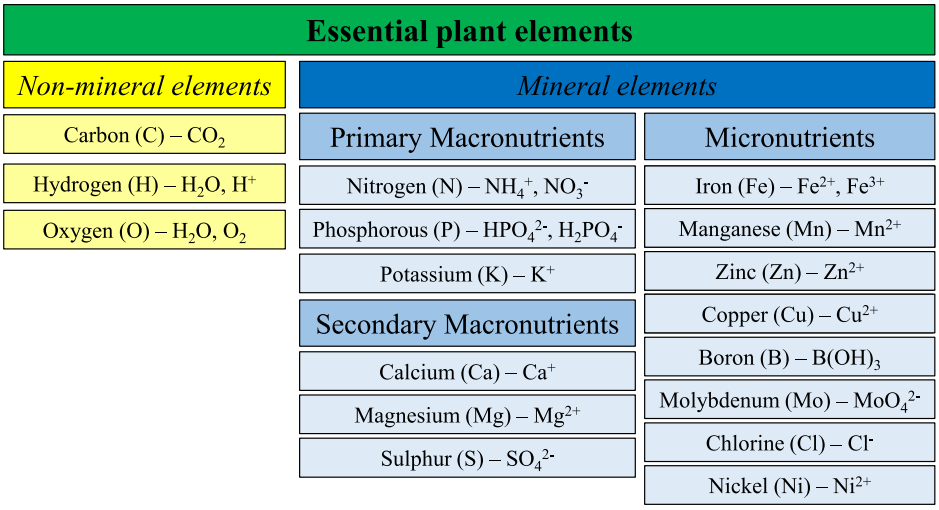

FIGURE 9. Essential nutrients required for plant growth and their available form in soil.

or in the form of natural biomass or water. The mineral elements that are required in relatively larger quantities for crop growth are categorized as primary macronutrients that includes N, P and K. The deficiencies in N, P and K may lead to significant yield losses and are therefore added exogenously to soil to meet the plant's needs. Ca, Mg and S are classified as secondary macronutrients as they are needed in relatively lesser amounts and are often present in sufficient quantities in soil. Plants also need other nutrients for healthy growth but only in trace amounts, these elements are classified as micronutrients. Micronutrients are largely present naturally in adequate amounts in soil and if required, are added to macronutrient doses in minute quantities. Excessive concentrations of micronutrients in soil can also lead to toxicity in plants.

Nutrient/fertilizer application is one of the largest expenses incurred in crop production not only in terms of direct capital but also in terms of its ultimate impact on the environment. Hence, precise monitoring of nutrients in soil enables better application efficiencies and enhanced sustainability in agriculture. This section presents the methodologies employed towards detection of nutrients in soil, particularly primary macronutrients, and is divided into the following subsections:

- Laboratory-based methods,
- Ion-selective membrane (ISM)-based electrochemical (EC) sensors,
- Other biosensing methods, and
- Electrophoresis-based methods.

A. LABORATORY-BASED METHODS FOR SOIL NUTRIENT ANALYSIS

Standard soil testing procedures in laboratory (lab) setting consists of two main steps, (i) Sampling, and (ii) Nutrient extraction and quantification. Recommendations for soil sampling procedures vary with different laboratories [74]–[76]. In general, a large field can be divided into smaller areas of ∼20 acre, within which at least 15 to 20 soil cores from different locations (zig-zag pattern or randomized pattern etc.) can be taken at soil depths of 6 to 24 inches. The top six inches of soil has the most root activity and fertilizer applications are generally restricted to this depth, however, in case of deep rooted crops such as wheat or for more detailed nutrient analysis, cores from 6 to 24 inches can be taken. A relation between the number of cores and coefficient of variation is described in [77] and as expected, the variation decreases with larger number of collected sample cores. The collected soil samples are dried, ground and sieved prior to analysis to obtain a homogeneous mixture. To begin analysis, first the nutrients are extracted from the processed sample. The extractants are chemically separated from the sample to rapidly assess either total and/or available (or soluble) soil nutrient pools. Several nutrient specific extraction chemistries, often dependent on pH of the soil, have been developed over the years, such as *N* extraction using calcium sulphate, *P* and *K* extraction using Mehlich 3 method and more [76].

Colorimetry used to one of the standard laboratory soil testing methods prior to using more sophisticated instruments. In this method, the changes in intensity of color or turbidity is recorded in response to reactions between the sample extractant and a prescribed reagent, which directly correlates with the concentration of a specific ion. Various colorimetric reagents have been developed for detecting different soil nutrients, such as NO_3^- detection using diazotize dye method after conversion to nitrite using cadmium, NH_4^- detection using Nessler reagents, P using stannous chloride method, K by tetraphenylboron precipitation, Ca and Mg by ethylenediaminetetraacetic acid (EDTA) titraion and more [78]. The developed color is compared to a reference color strip according to which the concentration levels are determined. Thus the

accuracy of measurement is affected by the limited number of reference levels as well as human interpretation. However, in recent years, photometers and image processing has been applied for improved color analysis. A portable colorimetric analyzer based on smartphone camera for P determination in soil was presented in [79]. Colorimetric test kits are also readily commercially available providing low-cost per test for soil analysis [78], [80]. In general, colorimetry-based methods require several sample preparation steps making the process labor as well as time intensive.

Compared to colorimetry, *spectroscopy*-based methods offer more precise and rapid analysis with relatively simpler soil preparation requirements. Spectroscopic techniques like visible (vis), ultraviolet (UV) and IR spectroscopy, X-ray fluorescence (XRF) spectroscopy, inductively coupled plasma spectroscopy, among others, have been employed for laboratory-based soil testing. vis and UV spectrophotometers work on the principle of interaction of vis or UV light with the electron in the constituent atoms, where the electrons in orbitals can absorbs photons of specific energy (or wavelength) and are observed in the absorbance spectrum. Absorbance (*Abs*) at a particular wavelength can be related to the concentration of the analyte molecule using the Beer-Lambert law as:

$$Abs = \alpha \times l \times C_0, \tag{18}$$

where α is the absorption coefficient, l is the path length of light through the sample, and C_0 is the concentration of the analyte. α and l are constant for a given system and element, hence a direct relationship between absorbance and C_0 can be established [77].

In *IR spectroscopy*, the test sample is irradiated with IR radiation and the frequencies corresponding to the vibrational modes of the atomic/molecular bonds are absorbed while the rest are reflected. The output spectrum is recorded using a spectrophotometer where different molecular bonds exhibit distinct vibrational modes which are characterized in the IR absorbance bands.

In *inductively coupled plasma (ICP)* optical emission spectroscopy (ICP-OES), the test samples are introduced inside the core of ICP argon plasma which generates temperature of about $8000^\circ\ C$ making the thermally excited elements emit light at their characteristic optical wavelengths. The emitted light is scanned using a spectrometer and the amplitude at each wavelength is recorded is representative of the elemental concentration [81].

XRF spectroscopy works on the principle that when primary x-rays are targeted at a sample, secondary x-radiation (fluorescence) is emitted by the target. Electron bombardment at the target can also be used as a source of primary excitation. When excited, each element emits x-rays of characteristic wavelength (inversely related to the square of the atomic number of the element) and intensity, proportional to the amount of the element present [82].

Soil testing in labs currently cost between \$8 to \$25 per test per sample depending on the information required, and are typically performed on an average every 3 to 5 years [74], [75]. Laboratory- based methods provide accurate as well as precise measurements which are used as standard (or ground truth) for other sensing techniques but require several sample collection and preparation steps. Therefore there exists a need for cost-effective and field accessible soil nutrient sensing technologies to enable continuous monitoring for precise fertilizer application as well as soil health analysis. Subsequent sections discuss various sensing technologies developed and applied towards soil nutrient analysis with the potential for providing portable, accurate, quick, continuous and low-cost measurements.

B. ION-SELECTIVE MEMBRANE (ISM)-BASED ELECTROCHEMICAL METHODS

Sensors like ion selective electrodes (ISEs) and ion selective field-effect transistors (ISFETs) use ion selective membrane (ISM) for selectivity and are the most common electrochemical sensing methods studied and applied for the determination of inorganic ions in soil. ISMs can be classified into 3 broad categories: (i) glass membrane (primarily used for pH measurement), (ii) inorganic salt crystal-based solid state membranes, and (iii) polymer membranes containing ionophores. This last kind (a polymer ISM) is typically made from a mixture of the ionophore/ligand, a high molecular weight polymer matrix as the base material for ionophore immobilization, and a platicizer that imparts flexibility as well as enhances dissolution of the ionophore in the polymer. Often an anion or cation exchanger is added to the mix which may improve the selectivity of the membrane. Synthesis of ISMs developed for detecting various anions and cations can be found in [83]. A general procedure for fabricating ISMs includes pouring the prepared recipe in a glass mold, kept in an air permeable enclosure, until the solvent evaporates and the ISM is left behind for use [84].

The detection principle of an ISE is based on a potentiometric electrochemical (EC) cell where instead of direct analyte redox reactions, selective binding of the analyte ion to a membrane generates an electric potential. An ISE sensor is composed of a complete galvanic cell with two electrodes, a working electrode (WE) and a reference electrode (RE), where an ISM specific to a particular analyte/ion is integrated with the WE, and the potential difference between the WE and the RE varies depending on the concentration/activity of the analyte in the test solution/electrolyte. Figure 10 shows the general construction of ISE devices, where the conventional ISE (C-ISE) of Figure 10(a) is composed of a working electrode (WE) in an internal reference solution inside a glass tube interfaced with the test solution via the ISM, and a reference electrode (RE) with a porous frit. In contrast, a solid state (or solid contact) ISE (SS-ISE) of Figure 10(b) is made of a solid state RE, together with a metallic electrode coated with an ISM serving as the WE. Often there is an ion-to-electron transducer material sandwiched between the bare metal and the ISM. As the term suggests, the RE is a non-polarizable electrode, which means that its cell potential

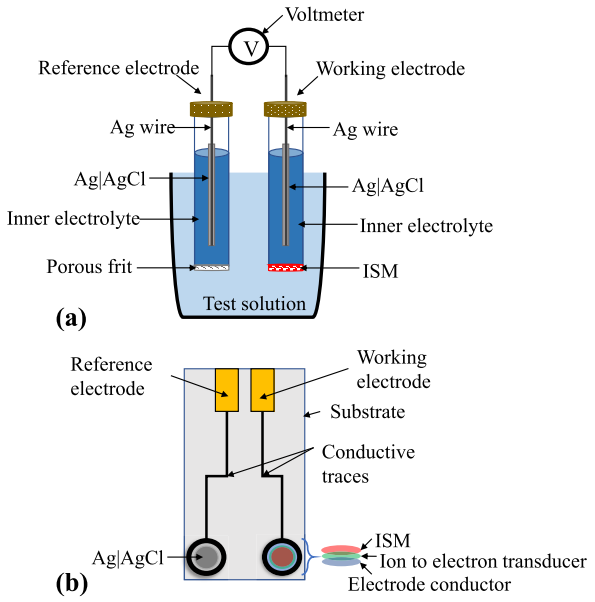

FIGURE 10. **(a) Schematic of a conventional ISE. (b) Schematic of a planar all solid state ISE.**

in a suitable electrolyte remains unchanged, hence can be used as a reference potential/ground. A commonly used RE in EC sensing is formed using a silver wire coated with silver chloride (Ag/AgCl) kept in chlorinated (saturated potassium chloride) solution/electrolyte as depicted in Figure 10(a). A general chemical structure of a C-ISE cell with Ag/AgCl reference electrodes can be given by:

$$Ag(s)|AgCl(s)|Cl^{-}(aq)||A^{+}(aq, sample)|ISM|A^{+}(aq, inside), Cl^{-}|AgCl(s)|Ag(s), \quad (19)$$

where || represents physical separation between chemical species via a porous membrane or frit, | represents separation of chemical species in different phases, **ISM** represents separation by an ISM, and A^{+} is the analyte ion of interest (assumed to have a unit positive charge).

When a conventional ISE as denoted by (19) is immersed in the test solution, then based on the concentration difference, the analyte ion diffuses across the ISM which creates ionic charge difference across the membrane surfaces. The inner reference electrode system constituting the WE acts as a transducer and converts the ionic charge difference into electronic charge through a reference redox reaction ($AgCl(s) + e^{-} \rightleftharpoons Ag(s) + Cl^{-}$), leading to a potential difference between the WE and the RE, E_{ISE}, given by the well known Nernst equation as:

$$E_{ISE} = E_0 + \frac{RT}{zF} ln\left[\frac{a_{(sample)}}{a_{(inside)}}\right] \Leftrightarrow E_{ISE} = E_0 - \frac{RT}{zF} ln[a_{(inside)}] + \frac{RT}{zF} ln[a_{(sample)}], \quad (20)$$

where E_0 is a reference potential under standard conditions (and is a constant for a given ISE structure), R is the gas constant (8.314 J mol^{-1} K^{-1}), T is the temperature in °K, F is the Faraday constant (96485 C/mol), z is the charge on the analyte ion, $a_{(sample)}$ is the ionic activity (or concentration) of the analyte in the test solution, and $a_{(inside)}$ is the known ionic activity (or concentration) in the inner electrolyte.

In practice however, the ISM may respond to some interfering species in the solution, hence the overall measured electric potential difference can be given by the Nikolskii-Eisenman form of the Nernst equation [85] as:

$$E_{ISE} = E_0 - \frac{RT}{zF} ln[a_{(inside)}] + \frac{RT}{zF} ln[a_{(sample)} + \sum K_j (a_j)^{z/z_j}], \quad (21)$$

where a_j is the activity/concentration, z_j is the charge, and K_j is the selectivity coefficient of the j^{th} interfering ion. (20) and (21) describe the logarithmic relationship between the electric potential and the ionic activity/concentration which is representative of potentiometric EC sensors like ISEs.

Although functional and accurate, there are challenges associated with conventional ISEs (C-ISE) in terms of durability, leakage/contamination of inner solutions, difficulty in miniaturization and portability. Solid-state ISEs (SS-ISE) were developed to overcome the drawbacks of the C-ISEs. However, SS-ISEs often encounter potential drift due to inner aqueous layer formation change in chemical composition, which may be improved through electrode conditioning [86]. The earlier versions of the SS-ISE used direct contact electrodes also known as coated wire electrodes (CWE) where an ISM layer was directly attached on a metallic surface without any inner filling solutions, but this exhibited high interface resistance leading to potential instability and problems in reproducibility [87]. In order to improve the operation of SS-ISEs, ion-to-electrode transducer materials were introduced between the metallic surface and the ISM. Various ion-to-electron transducer materials have been explored in literature such as hydrogel layers and conductive polymers which operate similar to the inner electrode by undergoing redox reaction in the hydrogel or polymer matrix itself [88].

Apart from ISEs, transistor-based ISFET sensors have also been developed as shown in Figure 11. These have the same basic construction as the well-known metal-oxide-semiconductor field effect transistor (MOSFET) devices where the current flowing between the source and drain terminals is controlled by the voltage on the gate terminal. The general expression for the drain current (I_d) for a MOSFET is given by:

$$I_d = \frac{1}{2}\mu_{n/p} C_{ox} \frac{W}{L}[2(V_{gs} - V_T)V_{ds} - V_{ds}^2], \quad (22)$$

where $\mu_{n/p}$ is the mobility of the electrons/holes depending on the device type, N-channel or P-channel MOSFET, C_{ox} is the gate oxide capacitance, V_{gs} is the potential difference between gate and source, V_{ds} is the potential difference between drain and source, V_T is the threshold voltage for the inversion layer to form in the channel, and W and L represent the width and the length of the channel, respectively. The

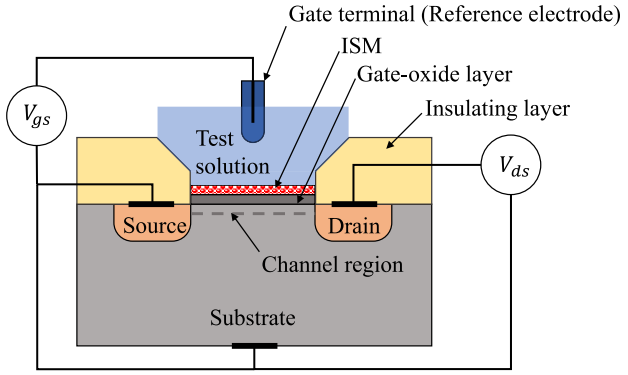

FIGURE 11. A schematic of an ISFET sensing device.

gate region is coated with the ISM and is exposed to the test solution. A RE in the solution is used as the gate terminal with respect to which V_{gs} is applied. The ISM only allows specific ions to accumulate electrostatic charge on the gate, affecting the overall V_T (determined as the potential value in (20)), resulting in the change in the drain current according to (22).

1) N DETECTION USING ISMs

Plants take majority of N from soil in the form of NO_3^-, however NH_4^+ can be dominant in some acidic and/or anaerobic environments, and it has been widely accepted that co-provision of nitrate with ammonium may be ideal for plant growth [98]. Among the inorganic forms of N, nitrate is the most mobile making it prone to leaching and therefore, requires frequent replenishment. The ideal concentration range of nitrates in soil is about 10 to 30 mg/kg or approximately 0.1 to 0.5 mM [99], which coincides with the detection range of most ISM-based devices.

N detection using ISEs and ISFETs has been explored for several decades and many recipes have been developed for nitrate ISMs. In one of the prominent early works on nitrate ISE (1976), a series of symmetrical quaternary ammonium compounds were synthesized, purified and tested as ligands in various plasticizers, and polyvinyl chloride (PVC) to form non-porous PVC-membrane-based ISEs. A combination of ionophore tetradodecylammonium nitrate (TDDA), plasticizer dibutylphthalate (DBP) in PVC polymer matrix with the composition of 4% TDDA, 67% DBP, and 29% PVC was proposed as optimal [100]. The developed sensor exhibited a sensitivity of 56.2 mV/decade with the limit of detection of 8.3×10^{-7} M and $\ln(K_j)$ values for Cl^-, NO_2^-, F^- and HCO_3^- as -2.30, -1.15, -3.0 and -3.30, respectively.

Since then many nitrate selective membranes have been reported in literature [83], [99] with various objectives including, improving selectivity with respect to interference from Cl^- [85], [101], developing portable inexpensive devices and improving potential stability in SS-ISEs [93]. The sensors exhibit near-Nernstian slope; Nitrate ion has a unit negative charge (or $|z| = 1$), and hence according to (21), the theoretical Nernstian-slope (RT/zF) magnitude or sensitivity for NO_3^- ion is $\sim$ 59.2 mV/decade. In general, the ISE sensing technology for N detection have matured successfully in the past decades offering reliable commercial products, often used as standard for in-field testing as well as in lab testing, however, new devices with unique characteristics like low cost fabrication, longer life times, continuous use with easy, robust and quick operation are being developed continually. Table 2 presents a brief overview of some of the recent ISM-based devices used for detecting nitrate in soil media.

Among recently reported works, laser induced graphene (LIG) electrodes were fabricated on polyimide/Epson printer paper and were functionalized with ionophores, tridodecylmethylammonium nitrate and nonactin within PVC-based membrane to form solid contact (SC) ISEs for NO_3^- and NH_4^+ detection, respectively [94]. The LIG SC-ISEs displayed near Nernstian sensitivities of 51.7 $\pm$ 7.8 mV/dec and 54.8 $\pm$ 2.5 mV/dec, and detection limits of 28.2 $\pm$ 25.0 μM and 20.6 $\pm$ 14.8 μM for NH_4^+ and NO_3^-, respectively. Soil slurry sensing was performed, and recovery percentages of 96% and 95% were obtained for added NH_4^+ and NO_3^-, respectively.

Another work demonstrated a low-cost and flexible SS-ISE using inkjet-printing for in-field nitrate detection, where the effect of ISM film thickness was studied with the conclusion that thicker ISM leads to longer conditioning requirement but smaller drift [90]. The developed ISEs (irrespective of thickness) presented 50-52 mv/dec sensitivity in a wide range of 0.0001 M to 0.1 M nitrate and about 95% accuracy in soil nitrate detection.

A novel nanocomposite of poly(3-octyl-thiophene) and molybdenum disulfide (POT-MoS_2) was reported as an ion-to-electron transducer with high hydrophobicity (minimizing the formation of thin water layer at the electrode interface) and redox properties for nitrate SS-ISE [91]. Tridodecylmethylammonium nitrate-based ISM with the proposed ion-to-electron transducing layer coated on Au electrode (100 nm Au deposited on copper on a PCB substrate) was used, resulting in the detection range of 1-1500 ppm with sensitivity of 64 mV/decade, and exhibited a life time of 27 days of continuous use in monitoring nitrate in soil slurry.

Alternatively, ionic-liquid (IL)-based ISMs have also been studied for N detection. ILs are specific salts generally composed of two asymmetrical ions of opposite charge (usually big organic cations and smaller anions), and possess unique properties, such as low volatility, tunable viscosity, high conductivity, large electrochemical window [95]. The use of IL/water two-phase system appears to be very promising for electroanalytical chemistry, where ILs have been successfully utilized as almost any major component of ISEs (ionophore, ion exchanger, plasticizer) [92]. A multi-functional usage of ionic liquid trihexyltetradecylphosphonium chloride (THTDPCl) for the preparation of PVC-based polymeric membrane solid contact nitrate ISE was reported with the sensitivity of 60.1 mV/decade and the detection range of 10^{-5} M to 10^{-1} M [95]. However, it was observed that chloride ion concentrations about 1 mM can interfere with nitrate

TABLE 2. Brief comparison of recent ISM-based EC devices for N detection.

Device type	ISM description	Sensitivity (mV/decade [ISE])	Linear detection range (M)	LOD[a] (μM)	Comments	Ref., Year
ISE	Nitrate doped polypyrrole (PPy(NO_3^-)) with a nanohybrid composite mediate layer of electrochemically reduced graphene oxide and gold nanoparticles (ERGO/AuNPs)	51.1	$10^{-5}-10^{-1}$	6.3	all solid state device with lifetime of 65 days, moderate interference from Cl^-, 10 s response time	[89], 2020
ISE	Tetra-n-octylammonium bromide (TOA-bromide), di-n-butylphthalate (plasticizer), PVC and tetrahydrofuran (THF) with ratio of PVC/TOA-bromide as 12:1 w/w and PVC/plasticizer/THF as 20/40/120 w/w/w	50–52	$10^{-5}-10^{-1}$	-	inkjet printed SS-ISE, effect of ISM thickness was studied (thicker film required more conditioning but showed smaller drift), comparatively higher interference from Cl^- was observed	[90], 2019
ISE	Methyltriphenylphosphonium bromide (0.25 wt%), nitrocellulose (moistened with 2-propanol (35%); 1.93 wt%), 2-nitrophenyl octyl ether (16.25 wt%), PVC (5.75 wt%), THF (74.3 wt%), and tridodecylmethylammonium (TDMA) nitrate (1.50 wt%)	64	$10^{-5}-10^{-2}$	~ 21	a novel nanocomposite of poly(3-octyl-thiophene) and molybdenum disulfide (POT-MoS_2) was used as ion-to-electron transducing layer coated on a patterned Au electrode, a lifetime of 27 days reported	[91], 2019
ISE	Phosphonium-based ionic liquid (plasticizer) with poly(methyl methacrylate)/poly(decyl methacrylate) (MMA-DMA) copolymer membrane-based ISEs selective for NO_3^- (ionophore free) and NH_4^+ (ionophore, Nonactin)	-	$5\times10^{-5}-5\times10^{-2}$	11.3	graphite pencil drawn electrode, tested against colorimetric assay exhibiting good correlation, explored phosphonium-based ionic liquid and MMA-DMA copolymer as an alternative for PVC	[92], 2018
ISE	1.1% (w/w) nitrate ionophore V, 0.7% (w/w) TDMA chloride, 65% (w/w) 2-nitrophenyl octyl ether (o-NPOE) and 33.2% (w/w) PVC	58.47	$10^{-5}-10^{-1}$	~ 1.6	Explored TTF-TCNQ[b] as ion-to-electron transducer, SS-ISE, improved potential stability, good selectivity	[93], 2018
ISE	0.25% (wt) methyltriphenylphosphonium bromide, 1.93% (wt) nitrocellulose dissolved in 35% 2-propanol, 16.25% (wt) 2-nitrophenyl octyl ether, 5.75% (wt) PVC, 74.32% (wt) THF, and 1.5% (wt) TDMA nitrate	54.8	$10^{-5}-10^{-1}$	20.6	Laser induced graphene (LIG) electrodes were printed on polyimide paper, ionophores functionalized for both NO_3^- and NH_4^+, low-cost disposable platform	[94], 2018
ISE	5% wt. trihexyltetradecylphosphonium chloride (ionic liquid) , 33%wt. PVC and 62%wt. 2-Nitrophenyl octyl ether (plasticizer)	60.1	$10^{-5}-10^{-1}$	2.8	Ionic liquid was explored as an ionophore, good sensitivity was observed, but with interference from chloride ions, if present above 1 mM concentration	[95], 2014
ISE	commercial grade ISE nitrate sensor (polymer membrane)	-	$7\times10^{-6}-1$	-	costs \$1,105.00, good detection range, based on C-ISE, requires maintenance	[96]
ISE	commercial nitrate ISE sensor	56	$1.5\times10^{-5}-0.2$	-	costs \$219.00 (sensor electronics not included), based on C-ISE	[97]

[a]LOD = Limit of detection
[b]TTF-TCNQ = Tetrathiafulvalene - 7,7,8,8-tetracyanoquinodimethane,

determination. Another recent work explored phosphonium-based ILs and poly (methyl methacrylate)/poly(decyl methacrylate) (MMA-DMA) copolymer as matrix materials alternative to classical PVC-based membranes in ISEs for NO_3^- and NH_4^+ detection [92]. Graphite pencil drawn electrodes were used for NO_3^- (ionophore free) and NH_4^+ (ionophore, Nonactin) detection, and demonstrated functionality by analyzing 8 water and 15 soil samples. A comparison of results using ISEs and colorimetric assay showed excellent correlation (Pearson's $R = 0.97$ and 0.99 for NO_3^- and NH_4^+, respectively).

2) P DETECTION USING ISMs

After N, P is the second most limiting primary macronutrient which is often supplemented in soil with external fertilizer application. It is absorbed by the plants largely in orthophosphate forms $H_2PO_4^-$ or HPO_4^{2-} present in soil. The fraction of these ions depend on the pH of the soil: For pH values above 7, HPO_4^{2-} is dominant whereas below pH 7, $H_2PO_4^-$ is abundant. Therefore, majority of ISE sensors have been reported for detecting these forms of phosphates. In soil extractants typical concentration of plant soluble phosphates range from 9 mg/kg to 30 mg/kg or 90 μM to 300 μM [111], which lies within the operation range of most of the ISM-based P sensing devices.

The selectivity of an ionophore towards an ion is governed by the hydration energy of the ion which is a measure of the free energy of transfer from the solution to the membrane phase, resulting in the Hofmeister series (perchlorate > thiocyanate > iodide > nitrate > bromide > chloride > acetate > phosphates) [112]. Phosphates have high hydration energy and consequently lie at the lower end of the Hofmeister series, this makes developing phosphate selective ionophores challenging. However, ISM-based sensors for P

TABLE 3. Brief comparison of recent ISM-based EC devices for P detection.

Device type	ISM description	Sensitivity (mV/decade [ISE]) or (μA/cm^2/mM [ISFET])	Linear detection range (M)	LOD (M)	Comments	Ref., Year
ISE for PO_4^{3-}	Molybdenum (Mo) blue electro-deposited on pencil graphite electrode with PVC coating	-	2.5×10^{-8} – 10^{-6}	$10^{-7.7}$	Based on electro-oxidation of Mo blue in the presence of PO_4^{3-} in acidic medium, showed good selectivity against NO_3^- and Si^{4+}, response degraded by 10 % after storing for 30 days at room temperature	[102], 2019
ISE for $H_2PO_4^-$	Nickel oxide/oxyhydroxide-modified printed carbon electrode (NiO/NiOOH-PrC), where NiOOH reacts with $H_2PO_4^-$ to form $NiPO_4$	78.48	$10^{-6} - 10^{-1}$	10^{-6}	SS-ISE, examined sensitivity for interfering ions: Cl^-, NO_3^-, SO_4^{2-}, Br^-, $H_3C2O_2^-$, and CO_3^{2-} as 2.56. 2.21, 9.23, 0.84, 1.04 and 6.13 mV/dec, respectively, usability confirmed over a period of 21 days	[103], 2019
ISFET for PO_4^{3-}	Nozzle jet printed silver/reduced graphene oxide (Ag/rGO) composite-based ISFET	62.2	$5 \times 10^{-6} - 6 \times 10^{-3}$	$10^{-6.7}$	based on the formation of Ag_3PO_4 on the electrode in the presence of PO_4^{3-}, exhibit under 5% variation from tested interfering ions, stable operation recorded for up to 4 weeks	[104], 2019
ISE for $H_2PO_4^-$	Based on consumption of surface cobalt (II) oxide layer to form cobalt phosphate compound	-	$10^{-6} - 10^{1}$	-	Evaluated with Ag/AgCl RE and Pt wire quasi-RE, Pt wire showed quicker response, sensor was validated with ICP-OES	[105], 2018
ISE for $H_2PO_4^-$	Coated cobalt wire electrode	39	$10^{-5} - 10^{-1}$	-	CWE-based sensor for $H_2PO_4^-$ in pH range 4 to 7, moderate selectivity, stable for 4 weeks in a hydroponic system	[106], 2018
ISE for HPO_4^{2-}	Ionophore Cu C,C,C,C-tetra-carboxylic phthalocyanine-acrylate polymer adduct (Cu(II)TCPc-PAA) fucntionalized on solid-state Si_3N_4 capacitor	27.7	$10^{-10} - 10^{-5}$	10^{-9}	a newly synthesized copper phthalocyanine ionophore was tested in a capacitive structure, wide detection range, moderate selectivity	[107], 2017
ISE for PO_4^{3-}	Based on the redox reaction between phosphate ion and molybdate ion in acidic media	-	$4 \times 10^{-6} - 3 \times 10^{-4}$	$10^{-5.4}$	inexpensive reagentless paper-based sensor	[108], 2016
ISE for HPO_4^{2-}	Cu monoamino phthalocyanine covalently attached to poly (n-butyl acrylate) ionophore (14.31%), benzyl-dimethylhexadecyl ammonium chloride as lipophilic cationic additive, conducting polymer PEDOT[c] as ion-to-electron transducer	29.8	$4 \times 10^{-9} - 1 \times 10^{-2}$	10^{-9}	Solid contact gold electrode was functionalized, ionophore composition in ISM was tuned to achieve desired selectivity, potential drift due to aqueous layer formation observed	[109], 2016
ISE for HPO_4^{2-}	1,8-Anthracenemethanamine (8.0 wt%) ionophore, o-NPOE (58 wt.%) plasticizer, PVC (32 wt.%) membrane matrix and TDMA chloride (2 wt.%)	30.8	$10^{-7} - 10^{-3}$	10^{-7}	SS-ISE with response time of about 10 s and life time of $8 - 9$ weeks, selectivity coefficients ($\ln(K_j)$) for OAc^- -2.4, NO_3^- -2.0, ClO_4^- -2.7, Cl^- -1.8, I^- -2.3, and SO_4^{2-} -1.3 observed	[110], 2013

[c]PEDOT = poly (3,4-ethylenedioxythiophene)

have been reported in literature and the developed approaches can be classified into two broad categories: (i) polymer membrane-based electrodes containing organic ionophores, and (ii) metal compound-based electrodes. Table 3 presents a brief comparison of some of the key recent ISM-based sensors developed for determination of phosphates.

Among prominent earlier works on organometallic ionophores, binuclear organotin compound-based ionophores were shown to hold promise for polymeric ISM-based phosphate detection [99]. A PVC membrane containing bis(tribenzyltin) oxide (ionophore), o-nitrophenyl octyl ether (plasticizer) showing near-Nernstian response for HPO_4^{2-} was reported with detection range of 5×10^{-6} M to 10^{-1} M and slope of -30.1 mV/decade [112]. Note that as HPO_4^{2-} has 2 units of charge (or $|z| = 2$), therefore according to (21), the theoretical Nernstian-slope (RT/zF) magnitude or sensitivity for this ion is $\sim$ 29.6 mV/decade. Since then, numerous other approaches have been reported for P detection and some of the recent works are discussed as follows.

A SS-ISE sensor for HPO_4^{2-} based on copper monoamino phthalocyanine (CuMAPc) covalently attached to poly (n-butyl acrylate) (PnBA) was reported in [109]. The SS-ISE was constructed by the application of a thin film of a polymer cocktail containing a CuMAPc–PBDA ionophore and benzyl-dimethylhexadecyl ammonium

chloride (BDMHAC) as a lipophilic cationic additive onto a gold electrode pre-coated with the conducting polymer poly (3,4-ethylenedioxythiophene) (PEDOT) as an ion and electron transducer. The sensor exhibited moderate selectivity with sensitivity of 29.8 mV/decade and a linear detection range of 4×10^{-9} M to 10^{-2} M. Selectivity coefficients ($\ln(K_j)$) for OAc^- −2.42, NO_3^- −2.13, ClO_4^- −3.89, Cl^- −1.85, I^- −1.96, F^- −2.98 and SO_4^{2-} −4.94 were observed.

In another work, an electrochemical capacitive sensor based on Al-Cu/Si-p/SiO_2/Si_3N_4 substrate functionalized with copper C,C,C,C-tetra-carboxylic phthalocyanine-acrylate polymer adduct (Cu(II)TCPc-PAA) ionophore was reported and tested in high (10 kHz) and low (100 Hz) frequencies using Mott-Schottky electrochemical technique [107]. A wide detection range from 10^{-10} M to 10^{-5} M with Nernstian sensitivity of 27.7 mV/dec was observed.

Electro-analytical reactions of phosphate ions with metallic compound electrodes can be characterized using EC methods and have been reported for developing ISEs for P detection. Coated cobalt metal wire electrode is one such device which have been extensively studied for detecting orthophosphates. A phosphate sensitive Co electrode for sensing $H_2PO_4^-$ in ammonium lactate-acetic acid soil extracts was reported, where the mechanism of detection was based on the conversion of surface cobalt oxide (CoO) to cobalt phosphate $Co_3(PO_4)_2$, and characterization using cyclic voltammetry (CV) [105]. Comparison was done between using Pt wire versus Ag/AgCl as RE, where Pt wire exhibited faster response and wider detection range. Soil samples were tested using the developed sensor and were in good correlation with ICP-OES. Another work based on the formation of $Co(H_2PO_4)_2$ in the coexistence of surface CoO and/or $Co(OH)_2$ on cobalt wire electrode was reported, where the selectivity coefficients ($\ln(K_j)$) for HCO_3^-, NO_3^-, CH_3COO^-, SO_4^{2-}, and Cl^- were evaluated to be −2.1, 2.5, −3.2, −4.0, and −4.0, respectively [106].

In another work, Molybdenum blue (Mo blue) was electrodeposited on a pencil graphite electrode (MB/PGE) by CV method between −0.5 and 1.0 V versus Ag/AgCl (3.0 M KCl) in a 0.5 M Na_2MoO_4 $2H_2O$ solution at 100 mV/s, and was used in the detection of phosphate ions [102]. PVC was used as a coating agent for the modified electrodes to improve their stability. Differential pulse voltammetry (DPV) was used to determine PO_4^{3-} content in soil samples, where the potential was scanned between −0.05 V and +0.15 V versus Ag/AgCl (3.0 M KCl) with a 10 mV/s scanning rate, and the peak currents were recorded around 0.06 V in acidic medium. The involved oxidation reactions in the presence of phosphate ions can be given by [102],

$$PO_4^{3-} + 12MoO_4^{2-}(Mo\ blue) + 27H^+ \rightarrow H_3PO_4(MoO_3)_{12} + 12H_2O \quad (23)$$

$$H_3PMo(VI)O_{40} + xe^- \Leftrightarrow [H_4PMo(VI)_8Mo(V)_4O_{40}]^{3-} \quad (24)$$

A paper-based screen-printed EC sensor working on the similar mechanism as described by 23 and 24 was developed where the electroactive area was modified with 100 mM molybdate ions, 100 mM KCl (supporting electrolyte) and 100 mM sulfuric acid, and the formation of phosphomolybdic complex in the presence of phophate ions [108].

Alternatively, a solid state sensor using nickel oxide-oxyhydroxide-modified printed carbon electrode for potentiometric phosphate detection was developed, where in alkaline media and in the presence of hydroxide groups, NiO (Ni(II)) is oxidized to NiOOH (Ni(III)) as an intrinsic redox processes, and in the presence of phosphate, NiOOH reacts with $H_2PO_4^-$ to produce nickel phosphate ($NiPO_4$) characterized using chrono-potentiometry [103]. Sensitivity of the developed sensor was examined towards the following interfering ions: Cl^-, NO_3^-, SO_4^{2-}, Br^-, $H_3C_2O_2^-$, and CO_3^{2-} with the recorded values of 2.56. 2.21, 9.23, 0.84, 1.04 and 6.13 mV/dec, respectively as compared to 78.48 mV/dec for $H_2PO_4^-$.

A nozzle-jet printed silver/reduced graphene oxide (Ag/rGO) composite-based ISFET sensor on a flexible disposable polymer platform was presented where the mechanism of the phosphate ion detection was elucidated as [104],

$$3Ag^+ + PO_4^- \rightarrow Ag_3PO_4 \quad (25)$$

The sensing mechanism was confirmed by performing X-ray photoelectron spectroscopy (XPS) analysis of the Ag/rGO ISFET. The selectivity and interference test of the Ag/rGO FET sensors was carried out towards interfering ions such as SO_4^{2-}, Mg^{2+}, K^+, HCO_3^-, Ca^{2+}, and thiamine pyrophosphate chloride (TPP) showing under 5% variation in phosphate detection.

3) K DETECTION USING ISMs

The interest in K detection spans from monitoring its levels in human serum [121] to determining its concentration in soil [115]. K is the third critical nutrient for crop production, and although it is present in the soil in large quantities, the plant available K pool is small [122]. Desired potassium ion levels in soil range from 50 mg/kg to 600 mg/kg or 1.25 mM to 15 mM [111]. Table 4 presents a comparison between the recent ISM-based sensors and devices for potassium-ion detection.

Among the ISMs developed for K detection, valinomycin has been observed to be the most successful ionophore for potassium ion detection because of its high selectivity towards the ion [99]. Recent advances in ISM-based K sensing have been towards developing low cost, and portable solid state devices for in-field applications. In one such work, a handheld device using screen-printed SS-ISE was presented, where a plasticizer-free butyl acrylate ISM, doped with ionophore valinomycin and lipophilic salt was deployed for detecting K in soil (extracted using strontium chloride) [115]. Carbon-nanotubes (CNT)-based ink was used to print WE and AgCl ink was used for printing RE before drop casting membranes (Polyvinyl butyral or PVB for RE) on the

TABLE 4. Brief comparison of recent ISM-based devices for K detection.

Device type	ISM description	Sensitivity (mV/decade [ISE]) or (μA/decade [ISFET])	Linear detection range (M)	LOD (M)	Comments	Ref., Year
ISE	Valinomycin (2 mg), potassium tetrakis 4-chlorophenyl borate (KTClPB) (0.5 mg), bis(2-ethylhexyl) sebacate (64.7 mg) plasticizer, and PVC (32.8 mg) in THF (1 ml)	53.34	$10^{-4.24}$ – 1	$10^{-4.24}$	ISM cocktail was drop-casted on the rGO/Au electrode, rGO was used as the ion-to-electron transducer improve the potential stability	[113], 2020
ISFET	22 mg of Potassium ionophore III[a] was mixed with 10 mg of the lipophilic salt KTClPB, 330 mg of PVC and 660 mg of dioctyl sebacate (DOS) plasticizer, all dissolved in 4 ml THF	6.58	10^{-9} – 10^{-2}	10^{-9}	Potassium ionophore III[a] decorated graphene ISFET, high resolution, moderate selectivity, good stability observed over a period of 5 months.	[114], 2019
ISE	12 mg valinomycin, 3 mg (KTpClB), 3 mg tetrakis(4-chlorophenyl)borate tetradodecylammonium salt (ETH500), and 7 mg 2,2-dimethoxy-2-phenylacetophenone (DMPP) dissolved in a stock mixture of 500 L butyl acrylate (BA) and 2 L hexane-1,6 diol diacrylate (HDDA)	61	10^{-6} – 10^{-2}	$10^{-5.2}$	Portable disposable screen printed SS-ISE with handheld reader, near-Nernstian sensitivity in the presence of a 0.02 M strontium chloride extraction solution, measured K in soil validated with ICP-atomic emission spectroscopy (R^2 = 0.89)	[115], 2018
ISE	1% valinomycin, 0.4% KTFPB, 32.9% PVC and 65.7% DOS, all in wt.%, after evaporation of the solvent THF	∼53	10^{-5} – 10^{-2}	$10^{-5.2}$	ISM coated over conducting polymer polypyrrole (PPy) with microporous zeolite as ion to electron transducer material, enhanced detection limit as compared to PPy(Cl^-)	[116], 2017
ISE	30 mL THF solution containing 1.1% (w/w) valinomycin, 0.25% (w/w) KTpClPB, 65.65% (w/w) o-NPOE, and 33% (w/w) PVC	59.1	$10^{-6.5}$ – 10^{-1}	$10^{-6.5}$	ISM was coated on a superhydrophobic graphene/carbon black nanocomposite enhancing the potential stability which was validated by 50 h of continuous K^+ monitoring	[117], 2015
ISE	Composition in w/w%: 1.0% valinomycin, 0.5% KTClPB, 65.2% DOS, and 33.3% PVC	59.2	$10^{-4.5}$ – 10^{-1}	10^{-5}	Graphene sheets used as transducer layer between valinomycin-based ISM and glassy carbon electrode, SS-ISE exhibited Nerenstian slope and a short response time of 10 s	[118], 2012
ISE	Commercial potassium ISE sensor	56	2.5×10^{-5} – 1	-	costs $219.00 (data logger not included), good operation range, based on C-ISE	[119]
ISE	Commercial grade potassium ISE sensor	-	10^{-6} – 1	10^{-6}	costs $1225.00, large operation range, based on C-ISE	[120]

[a]Potassium ionophore III = 2-Dodecyl-2-methyl-1,3-propanediyl bis[N-[5-nitro(benzo-15-crown-5)-4-yl] carbamate]

printed strip electrodes. A custom reader was also developed to measure the potential difference between the WE and RE pair enabling truly portable operation. The selelctivity coefficients ($\ln(K_j)$) were recorded for Na^+, Mg^+, Ca^{2+}, Li^+ and NH_4^+ as −2.6, −4.3, −4.7, −2.3 and −1.7, respectively.

In another work, reduced graphene oxide (rGO) was proposed as an ion-to-electron transducer for a screen printed SS-ISE-based K sensor [113]. Valinomycin-based ISM was drop-casted on to the surface of rGO/Au electrode, and rGO layer was shown to improve the potential stability by inhibiting the formation of thin water layer in the electrode surface. A potential reading circuit was developed on the PCB platform for portable operation. A superhydrophobic graphene/carbon black nanocomposite-based solid contact K-ISE was reported in [117], where a valinomycin-based ISM was coated on the superhydrophobic material. The developed sensor was characterized by cyclic voltammetry, chronopotentiometry and impedance spectroscopy, and exhibited large capacitance improving the long term potential stability of the ISE which showed about 1 μV/hr variation after 50 h of continuous use.

Although naturally occurring valinomycin offers superior selectivity and sensitivity, Potassium ionophore III (2-Dodecyl-2-methyl-1,3-propanediyl bis[N-[5'-nitro(benzo-15-crown-5)-4'-yl] carbamate]) has also been used for K-ISM fabrication as an alternative to valinomycin which is classified as a hazardous substance [114]. An ISFET device using potassium- ionophore-III-based ISM incorporated into parylene encapsulated graphene FET was reported in [114]. The fabricated device exhibited high resolution K sensing of the order of 1 nM. Moderate selectivity was observed with highest interference sensitivity of 9 mV/dec was recorded for NH_4^+ as compared to 37 for K^+. However, the developed sensor showed good correlation with a commercial K-ISE when testing K^+ levels in samples like milk, grape juice, lemon juice, bovine and sheep blood.

4) MULTI-MACRONUTRIENT SYSTEMS BASED ON ISMs

Multi-ion detection systems employing multiple ISEs have also been developed in literature. In one such recent work, an automated sensing platform for hydroponic macronutrients using an array of ISEs was reported [123].

Different PVC-based ISMs were prepared for detecting NO_3^-, K^+, Ca^{2+} and Mg^{2+}. Alternatively, low-cost disposable paper-based potentiometric ion sensing systems using ISMs for detecting K^+, NH_4^+, Na^+, Ca^{2+} and pH have also been developed [124], [125]. The sensors exhibit near-Nernstian sensitivity while operating in the concentration range of interest.

In another work, a piezoresistive microcantilever-based portable lab-on-a-chip sensing system for detection of macronutrients, NO_3^-, $H_2PO_4^-$, K^+, in the soil using ISMs was reported [126]. The developed piezoresistive silicon microcantilevers were coated with a polymer matrix containing ionophores; methyltridodecylammonium nitrate /nitrate ionophore VI, 18-crown-6 ether and Tributyltin chloride for NO_3^-, K^+, $H_2PO_4^-$, respectively. A microcantilever die consisting of an array of four microcantilevers was mounted on a PCB and contacts were made using either wire bonding or silver epoxy. A Teflon flow cell with inlet and outlet was placed on the PCB. Out of four microcantilevers, one was used as a reference and the other three were test cantilevers used for sensing. The reference and three different test microcantilevers functionalized with the coatings of N, P, and K will selectively bind different nutrients and will result in a change of resistance, which was measured using a Wheatstone's bridge-based portable electronic setup. Successful response was recorded for N and K with P to be tested in the future.

Overall, ISM-based sensors have been studied extensively and provide reliable detection for various applications including soil testing. Continuous progress in being made in improving the life time and the potential stability of low-cost SS-ISEs for quick in-field testing.

C. OTHER BIOSENSING METHODS

Besides ISM-based EC devices, other biosensors have also been reported for detecting macronutrients in soil, particularly N and P. Some of the key recent biosensing methods, including *enzymatic biosensors, molecularly imprinted polymer (MIP), aptamers, and electro-catalysis-based detection methods* are discussed in this section.

1) N DETECTION

The reduction of NO_3^- to NO_2^- in the presence of the enzyme, nitrate reductase (niR) can be characterized using EC methods to develop nitrate sensors. *Enzymes* are protein molecules that act as biological catalysts for specific biochemical reactions, and can thus, be used for developing selective and sensitive biosensors. In a recent work, a microfluidic impedimetric sensor for soil nitrate detection using graphene oxide (GO) and conductive nanofibers decorated with niR was reported [127]. The sensor was characterized using electrochemical impedance spectroscopy (EIS) and had a wide range of operation, 0.44 to 442 mg/L with the detection limit of 0.135 mg/L and sensitivity of 61.15 $\Omega/(mg/L)/cm^2$. In another work, an niR decorated extended-gate type organic FET-based enzymatic sensor for nitrate detection was reported, where a bipyridinium derivative was employed as an electron transfer mediator, and sodium dithionite served as electron donor to the enzyme in the solution phase [128]. The developed sensor exhibited a linear relationship was obtained in the region of the low concentration ($0 - 4.0 \times 10^-6$ M). Several other works have been reported on enzymatic (using niR) nitrate biosensors in the recent years on account of their excellent selectivity such as an intelligent portable biosensor usable for up to 10 days [129], a portable nitrate biosensing device using bi-modal approach combining EC and spectroscopy-based measurement [130], and amperometric nitrate biosensor based on CNT/PPy/niR biofilm exhibiting LOD, sensitivity and linear range of 0.17 mM, 300 nA/mM and 0.44mM to 1.45 mM, respectively [131].

In addition to enzyme-based approaches, MIP-based biosensing approaches such as described in [132] have also been reported, where Isobutyl nitrate (IBN) (1 mmol) and 1-allyl-2-thiourea (AT) (4.0 mmol) were used as template molecule and functional monomer, respectively. These sensors operate on the principle of selective binding of the analyte ion to the previously manufactured MIP molecules via dipole interactions and hydrogen bonding. The developed sensor was able to measure nitrate-N in the range 1 mg/L to 10 mg/L, and showed 6% and 4% variation against interfering Nitrite-N and sulphate ions, respectively as compared to 90% for nitrate. In another recent work, poly(N-methylpyrrole) imprinted with nitrate ions was evaluated and was found to exhibit lower dependence on pH as compared to PPy-based MIPs [133]. The developed sensor displayed a linear range of 5.0×10^{-6} M to 0.1 M nitrate with a near Nernstian slope of -56.3 mV per decade and a strong preference for nitrate ion. In general MIP-based sensors require relatively complex fabrication but offer better longevity, and stability as compared to other approaches.

Alternatively, the electro-reduction of nitrate to ammonium ion on copper-based electrodes (coated wire electrodes) has also been employed for nitrate detection. A composite of Cu nano-particles, multi-wall carbon nanotubes (MWCNT) and reduced-GO (rGO) for simultaneous electrochemical detection of nitrite and nitrate was reported in [134]. The electro-reduction of nitrate on Cu/MWCNT/rGO electrode was characterized using square wave voltammetry, the sensor demonstrated a detection range from 0.1 μM to 75 μM. In another work, Cu nanowires were used for the detection of nitrate in water exhibiting wide range, 8 μM to 5860 μM, when tested using differential pulse voltammetry (DPV) [135].

2) P DETECTION

An amperometric phosphate biosensor, based on a cobalt phthalocyanine screen-printed carbon electrode (CoPC-SPCE) employing enzyme pyruvate oxidase was reported in [136]. The principle of operation consisted of the enzymatic reaction in the presence of inorganic phosphate where pyruvate was converted to acetylphosphate, CO_2 and H_2O_2. The analytical response was then recorded by the electrocatalytic oxidation of the formed H_2O_2 with

Co^{2+} to produce Co^{+}. The developed sensor showed linear response in the range of 2.5 μM to 130 μM. In another work, a pyruvate oxidase (PyO)-based field-effect transistor biosensor was fabricated where PyO was functionalized on the ZnO nanorods (ZnO NRs) array grown on seeded SiO_2/Si substrate (gate region) providing high specific surface area [137]. The developed sensor exhibited sensitivity of 80.57 μA mM^{-1} in a wide linear range of 0.1 μM to 7.0 mM.

In another work, dual enzyme biochemistry was reported where phosphate determination is achieved by first, the enzyme purine nucleoside phosphorylase (PNP) catalyzed reaction of inosine and phosphate to produce hypoxanthine which is subsequently oxidized by the second enzyme, xanthine oxidase (XOx), first to xanthine and then to uric acid [138]. Both PNP and XOx are integrated in a redox active Os-complex modified polymer, which also acts as an ion-to-electron transducer. The developed bienzymatic cascade phosphate biosensor selectively delivers four electrons for each phosphate molecule present, and and additional two electrons from the electrochemical oxidation of uric acid either through $Os^{II/III}$-couple or O_2 directly at the glassy carbon surface. The developed sensor exhibited LOD of $\sim$0.35 μM.

Additionally, MIP-based sensors have also been developed for P detection where an interdigital capacitive biosensor using MIPs to detect phosphates in a hydroponic system was reported in [139]. MIPs were synthesized using functional monomers methacrylic acid (MAA) and N-allylthiourea, against the template molecules diphenyl phosphate, triethyl phosphate, and trimethyl phosphate. Selectivity of different MIPs were tested against nitrate and sulphate where a selective change in capacitance was observed for phosphate.

Fluorescence-based sensors have also been reported for P detection, where in one such work, synthesized thioglycolic acid (TGA) capped cadmium telluride (CdTe) quantum dots (QDs) were used in 'turn on' photoinduced electron transfer (PET)-based inorganic phosphate sensing in aqueous solution [140]. Europium (Eu^{3+}) was used as an intermediate species that quenches fluorescence of QDs (when excited with ultraviolet light of 375 nm), but with the addition of phosphate ions to the QD-Eu complex, the quenched fluorescence was recovered. This phenomenon was used to quantify fluorescence intensity with phosphate concentration in the solution. A non-linear calibration function was reported along with an interference study, showing moderate phosphate selectivity. In another work, a smartphone, paper-based fluorescent sensor for ultra-low inorganic phosphate detection was reported for P detection where a reflection-mode fluorescence-sensing apparatus was developed using the fluorophore, N-[2-(1-maleimidyl)ethyl]-7-(diethylamino)-coumarin-3-carboxamide (MDCC), bound to a bacterial phosphate binding protein to generate fluorescent optical signal proportional to the concentration of phosphate [141]. The developed sensor exhibited linear detection range from 1.1 to 64 ppb.

3) K DETECTION

K detection using EC sensors using ISM devices has been studied extensively with numerous commercial products for agricultural applications available in the market, see table 4, however, other biosensing strategies have also been developed where in a recent work, an aptamer-based sensor using the interaction of gold nano-particles (AuNPs) and a cationic dye for K detection was reported [142]. Aptamers are single-stranded functional oligonucleotides (DNA or RNA) which have been proved to have receptor-like activity and can display affinity for specific chemical species. In the developed framework, in the presence of K^+ ions, the aptamers dissociated from the surface of AuNPs (aptamer-modified AuNPs), and the free AuNPs and the cationic dye makes the solution green (due to aggregaton of AuNPs), therefore, the solution turns from orange to green as the concentration of K^+ increases. The linear range of the colorimetric paper sensor spanned from 10 μM to 40 mM and the detection limit of 6.2 μM was obtained with minimal variation in the presence of interfering ions.

In another work, a graphene Hall effect biosensor was developed for K detection where a flexible single-stranded DNA with guanine-rich sequences (5'-GGTTGGTGTGGTTGG-3') was immobilized on the graphene surface as a probe, which could fold into a tetraplex structure (guanine-quadruplexes) with K^+ ions due to the formation of intramolecular hydrogen bonding in order to efficiently and selectively capture K^+ ions [143]. Van der Pauw measurement configuration was used to test the sensor, and a linear detection range of 1 nM to 10 μM with LOD of 1 nM was observed. The developed sensor exhibited good selectivity except in case of Na^+ ions, where a variation of about 30% was recorded due to interference.

Alternatively, K^+ detection has also been realized using selective binding to fluorophore molecule and its characterization. In a recent work [144], a novel molecular K^+ probe for colorimetric, fluorescent, and photoacoustic detection was reported, where the developed probe called NK2 is composed of 2-dicyanomethylene-3-cyano-4,5,5-trimethyl-2,5-dihydrofuran (TCF) as the chromophore and phenylazacrown-6-lariat ether (ACLE) as the K^+ recognition unit. NK2 showed good response and high selectivity which was demonstrated by the absorbance spectrum, fluorescence spectrum, and photoacoustic measurements leading to a linear detection range of 5 mM to 200 mM.

D. ON-THE-GO SPECTROSCOPY-BASED METHODS

Besides extensive use in laboratory-based soil testing, spectroscopic methods have also been investigated for on-the-go soil nutrient sensing applications. A few of the key recent optical/spectroscopy-based sensing systems are presented here. A field mobile soil nitrate sensor using Diamond-Attenuated Total Internal Reflection Fourier Transform Infrared (D-ATR-FTIR) spectroscopy was reported in [145]. D-ATR-FTIR is similar to IR spectroscopy but instead of directly exposing the sample to the IR radiation,

the light is directed into a crystal placed in contact with the sample. The evanescent fields at the total internal reflection interfaces are characteristically attenuated at particular wavelengths, representative of the composition of the surroundings. An Agilent 4100 ExoScan (Agilent Technologies, Santa Clara, CA, USA) handheld spectrometer with a diamond ATR crystal was used for all spectral measurements exhibiting good accuracy for NO_3^- estimation.

In another work, a portable X-ray fluorescence (pXRF)-based nutrient analysis system with simplified sample preparation was reported [146]. Soil samples were tested in pellet or powder form using a commercial pXRF spectrometer, Tracer III–SD model (Bruker AXS, Madison, USA). Pressed pellet samples showed better response with moderate accuracy, with R^2 values for K and Ca as 0.87 and 0.78 respectively.

A portable soil nitrogen detector based on near-IR spectroscopy and using Back Propagation Neural Network (BPNN) was reported in [147]. Absorbance data was collected at six wavelengths (1550, 1300, 1200, 1100, 1050, and 940 nm) using the optical system consisting of six IR LEDs (one for each wavelength), shared drive circuit, optical fibers and a photoelectric sensor. The optical fibers used for directing light and recording absorbance were housed in a probe which was buried 30 cm under soil surface, and a micro-controller was used as a control unit. The collected data was then modelled using BPNN and demonstrated an R^2 value of 0.88.

Overall, on-the-go optical/spectroscopic methods for soil nutrient analysis offer fast and efficient measurements for single to simultaneous multiple ion detection. However, the accuracy is dependent on other factors such as soil particle size, organic matter, moisture content, environment temperature and surface roughness making the sample preparation procedure as well as data analysis method of critical importance.

E. ELECTROPHORESIS-BASED METHODS

Capillary electrophoresis (CE) works on the principle of physical separation of ions in a buffer solution traveling inside a capillary tube/microchannel under the effect of an electric field. A detector is located at the end of the tube or microchannel which records sequential crossing of the different types of ions. Following one of the early prominent works on zone electrophoresis in open-tubular glass capillaries [148], CE has progressed into an established contemporary analytical technique for quick high resolution sequencing of bio-molecules as well as inorganic ions. Most of the commercially available CE systems like [149], [150] are targeted towards bio-molecule detection costing $1000s and are limited to lab setting. However, recent advances have been made in the development of economical field-applicable CE systems for nutrient/inorganic ion monitoring in soil samples [151], [152].

Figure 12 shows the schematic operation of a CE-based sensing system. The separation of ions in CE method is

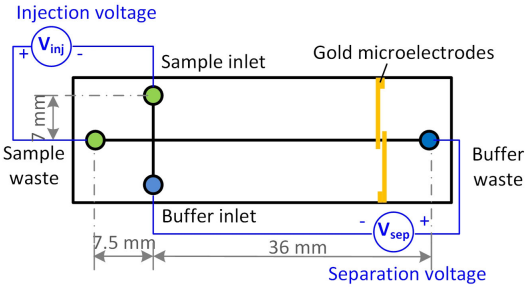

FIGURE 12. Schematic of a CE microchip ©[2017], IEEE [151].

based on their specific electrophoretic mobility when a potential difference is applied across the channel which results in the ions exhibiting unique migration velocity. Apart from the electrophoretic migration, ions also experience electro-osmotic forces due to the movement of the buffer solution through the capillary. This is caused by the charging of the capillary walls in the presence of an electric field and is dependent on the capillary material and pH of the buffer [153]. Therefore, the overall migration velocity (v_{net}) of an ion in a CE system can be given by,

$$v_{net} = (\mu_{EP} \pm \mu_{EOF})\bar{E}; \quad \mu_{EP} = \frac{q}{6\pi\eta r}, \tag{26}$$

where μ_{EP} is the electrophoretic mobility, μ_{EOF} is the mobility due to the electro-osmotic flow, $\bar{E}$ is the applied electric field, q is the ionic charge, η is the viscosity of the buffer solution and r is the radius of the ion. As shown in (26), μ_{EP} is a function of the ionic charge, ionic size and the viscosity of the buffer media as described by the well-known Stokes' law. Moreover, the electro-osmotic flow may hinder or enhance the mobility of the ion depending on the direction of the flow and the movement of the ion for a given electric field leading to a net migration velocity.

Several electrophoresis-based sensing systems for inorganic soil ion detection have been explored in the past including [153]–[155]. A brief review of the recent CE-based sensing systems applied towards soil nutrient ion measurement in the past decade is presented here. In a recent work, a nutrient sensing system using chip scale electrophoresis with in-situ soil extraction capability was reported in [151], [156]. The system is composed of a microfluidic electrophoretic chip with a two step process of ion detection. In the first step, an injection voltage (200V) is applied to load the sample in the channel from the sample inlet port, then a separation voltage (500V) is applied across the separation channel to segregate the ions. At the end of the separation channel, parallel electrodes measure the conductivity change across the channel, while the peaks corresponding to the ion concentration are detected at ion-specific time intervals. The system requires a few micro-litres of sample which is extracted from the soil using a vacuum pump coupled with a porous suction head and stored in a reservoir connected to the sample inlet port. The sensor was characterized for anions in soil including, Cl^-, NO_3^-, SO_4^{2-} and $H_2PO_4^-$ with a detection limit of $\sim 7.25\mu$M for nitrate ions. In another work, a lab-on-a-chip CE-based sensor was developed for detecting soil

nutrients [152]. The sensor used a microfluidic chips with channels of length of 44 mm and 64 mm, taking a curved route to accommodate the design on relatively smaller chip area. The injection voltage for loading a sample from the sample reservoir as well as the separation voltage across the channel were both 2000 V. The device was constructed using a glass substrate on which the electrodes were deposited through thermal evaporation, the channel was formed by selective lithography process with a photosensitive material, and then a polymethylmethacrylate (PMMA) top cover was bonded to seal the channel. Ion separation was shown for various soil nutrients but proper calibrations were done for NO_3^-, NH_4^+, PO_4^{2-} and K^+ exhibiting good linearity.

Compared to other methods, CE-based approaches has unique advantages such as simultaneous detection of multiple ions, minimal sample preparation and potential for developing fully in-situ long term nutrient monitoring systems. Whereas, high power requirement and use of moving parts that may need maintenance are some of the limitations of this method.

F. FUTURE PROSPECTIVE AND RESEARCH DIRECTION IN CROP NUTRIENT SENSING

On-the-go or in-situ sensing technologies will pave the way for future soil nutrient monitoring which in the present state are somewhat limited by sample collection and preparation requirements, and may not always be economical. Currently, soil nutrient determination is largely performed in laboratory setting which is not only expensive (per sample) but also time and labor intensive leading to irregular testings and low adoption rate. Depending on the application, from automated small scale green house farms to large crop growing operations, the need for easy to use, reliable and economical nutrient is immense. N, P and K are among the common externally supplemented nutrients making their efficient application in the field critical for both economical and environmental gains. Continuous progress is being made in various sensing methodologies as over-viewed in this article, ranging from low-cost solutions to portable and real-time applications while improving sensor lifetimes, selectivity, sensitivity and accuracy. Furthermore, future efforts may be directed towards validation and testing of crop nutrient sensing technologies in short and long term deployments in the field in order uncover and understand the effects of environmental factors on sensors enabling continuous in-field monitoring.

IV. SENSING IN AGRICULTURE: TRENDS AND FUTURE

With the growth in population and demand for agri-products, and the resulting ever increasing use of fertilizers and other agrochemicals in agriculture, monitoring nutrient levels in soil is becoming a critical need to ensure economic efficiency while minimizing the impact on environment. Precision agriculture through site specific management is emerging as a mainstream practice driven not only by environmental concerns but also by efficiency and profitability considerations, and enabled by the advances and adoption of technology in crop production. The market for precision agriculture is developing at a rapid pace, according to a recent report published by *Meticulous Research*, the global technology market in agriculture is expected to grow at a compound annual growth rate (CAGR) of 14.1% from 2019 to reach $34.9 billion by 2027 [157]. Sensor-based measurements form the basis for achieving sustainability through precision agriculture. Optimization of agricultural processes begins with data collection from sensors in soil, plant, air, and space, and analyzed using crop modeling software (for example [6]), to precisely tailor plant needs and manage crops. The availability of moisture and nutrients in soil is a critical determinant in crop growth and therefore, takes precedence when developing sensing technologies for precision agriculture. Overall, the trends in soil moisture and nutrient sensing are moving towards low-cost, easy to use, portable or field-deployable sensors providing sufficiently accurate data for precise soil and crop modelling leading to higher economical and environmental sustainability while improving the technology adoption rate in agriculture. While the progress on sensors based on different methods are being made, advances have also been made in their sensor-to-sensor networking through improved physical/MAC/Network layer designs for energy-efficient synchronization, scheduling, and routing [158], and also for network-based in-situ sensor position localization to aid their maintenance or replacement [159], [160].

V. CONCLUSION

This article presents an overview of soil moisture and nutrient sensing methodologies. Key soil moisture sensing methods spanning individual farmer's needs to more regional and large-scale soil management were discussed and compared, while the underlying principles of operations were explained in a concise manner. Besides soil moisture, brief description and comparison of the devised methods commonly applied for soil nutrient determination were also presented in this article. Based on the observed trends and needs, even though laboratory-based methods provide accurate measurements, the high cost and slow response times has instituted the need for quick on-the-go or in-situ sensors. Portable sensing systems with minimal sample preparation requirements have become the common goal for developing soil ion sensing technologies where effective site specific management can be realized accurately. Solid state devices on disposable platforms offer low cost measurements, whereas spectroscopic and CE-based methods offer the potential for continuous long term deployment in the fields. Overall, continuous developments are being made for monitoring soil properties accurately with the goal of making the technologies economical, and available leading to better resource management and sustainability in agriculture.

REFERENCES

[1] Population Division of the United Nations Department of Economic and Social Affairs. *World Population Projected to Reach 9.8 Billion in 2050, and 11.2 Billion in 2100*. Accessed: Jul. 19, 2020. [Online]. Available: https://www.un.org/development/desa/en/news/population/world-population-prospects-2017.html

[2] *Sustainable Agriculture Program | National Institute of Food and Agriculture*. Accessed: Jul. 19, 2020. [Online]. Available: https://nifa.usda.gov/program/sustainable-agriculture-program
[3] B. M. Campbell, D. J. Beare, E. M. Bennett, J. M. Hall-Spencer, J. S. I. Ingram, F. Jaramillo, R. Ortiz, N. Ramankutty, J. A. Sayer, and D. Shindell, "Agriculture production as a major driver of the earth system exceeding planetary boundaries," *Ecol. Soc.*, vol. 22, no. 4, pp. 1–11, 2017.
[4] M. M. Mekonnen and A. Y. Hoekstra, "Four billion people facing severe water scarcity," *Sci. Adv.*, vol. 2, no. 2, Feb. 2016, Art. no. e1500323.
[5] *RZWQM: USDA ARS*. Accessed: Aug. 10, 2020. [Online]. Available: https://www.ars.usda.gov/plains-area/fort-collins-co/center-for-agricultural-resources-research/rangeland-resources-systems-research/docs/system/rzwqm/
[6] A. Bhar, R. Kumar, Z. Qi, and R. Malone, "Coordinate descent based agricultural model calibration and optimized input management," *Comput. Electron. Agricult.*, vol. 172, May 2020, Art. no. 105353.
[7] M. Tuller and D. Or, "Water retention and characteristic curve," in *Encyclopedia of Soils in the Environment*, D. Hillel, Ed. Oxford, U.K.: Elsevier, 2005, pp. 278–289.
[8] T. J. Schmugge, T. J. Jackson, and H. L. McKim, "Survey of methods for soil moisture determination," *Water Resour. Res.*, vol. 16, no. 6, pp. 961–979, Dec. 1980.
[9] *Irrometer Sensors*. Accessed: Jul. 29, 2020. [Online]. Available: https://www.irrometer.com/sensors.html#irro
[10] *Soil Moisture Monitoring: A Selection Guide | Agriculture and Food*. Accessed: Oct. 10, 2020. [Online]. Available: https://www.agric.wa.gov.au/horticulture/soil-moisture-monitoring-selection-guide
[11] P. C. Dias, W. Roque, E. C. Ferreira, and J. A. S. Dias, "A high sensitivity single-probe heat pulse soil moisture sensor based on a single npn junction transistor," *Comput. Electron. Agricult.*, vol. 96, pp. 139–147, Aug. 2013.
[12] G. Ravazzani, "Open hardware portable dual-probe heat-pulse sensor for measuring soil thermal properties and water content," *Comput. Electron. Agricult.*, vol. 133, pp. 9–14, Feb. 2017.
[13] M. B. de Morais Franca, F. J. O. Morais, P. Carvalhaes-Dias, L. C. Duarte, and J. A. S. Dias, "A multiprobe heat pulse sensor for soil moisture measurement based on PCB technology," *IEEE Trans. Instrum. Meas.*, vol. 68, no. 2, pp. 606–613, Feb. 2019.
[14] ICT International. *Neutron Probe Smart503*. Accessed: Oct. 27, 2020. [Online]. Available: http://ictinternational.com/products/smart503/neutron-probe-smart503/
[15] W. Skierucha, A. Wilczek, A. Szypłowska, C. Sławiński, and K. Lamorski, "A TDR-based soil moisture monitoring system with simultaneous measurement of soil temperature and electrical conductivity," *Sensors*, vol. 12, no. 10, pp. 13545–13566, Oct. 2012.
[16] *Soilmoisture Equipment Corp:: Shop by Product:: Soil Moisture Meters:: Trase TDR Soilmoisture Meters:: Handitrase TDR Soilmoisture Meter W/FLD Probe*. Accessed: Oct. 29, 2020. [Online]. Available: http://www.soilmoisture.com/HT2/
[17] G. Pandey, R. Kumar, and R. J. Weber, "A low RF-band impedance spectroscopy based sensor for *in situ*, wireless soil sensing," *IEEE Sensors J.*, vol. 14, no. 6, pp. 1997–2005, Jun. 2014.
[18] Y. Kojima, R. Shigeta, N. Miyamoto, Y. Shirahama, K. Nishioka, M. Mizoguchi, and Y. Kawahara, "Low-cost soil moisture profile probe using thin-film capacitors and a capacitive touch sensor," *Sensors*, vol. 16, no. 8, p. 1292, Aug. 2016.
[19] *EC-5 | Soil Moisture Sensor | Meter Environment*. Accessed: Oct. 29, 2020. [Online]. Available: https://www.metergroup.com/environment/products/ec-5-soil-moisture-sensor/
[20] Spectrum Technologies. *Irrometer Tensiometers | Spectrum Technologies*. Accessed: Aug. 15, 2020. [Online]. Available: https://www.specmeters.com/soil-and-water/soil-moisture/tensiometers/tensiometers/
[21] *Irrometer Sensors*. Accessed: Jul. 27, 2020. [Online]. Available: https://www.irrometer.com/sensors.html#wm
[22] E. J. A. Spaans and J. M. Baker, "Calibration of watermark soil moisture sensors for soil matric potential and temperature," *Plant Soil*, vol. 143, no. 2, pp. 213–217, Jun. 1992.
[23] H. He, M. F. Dyck, R. Horton, T. Ren, K. L. Bristow, J. Lv, and B. Si, "Development and application of the heat pulse method for soil physical measurements," *Rev. Geophys.*, vol. 56, no. 4, pp. 567–620, Dec. 2018.
[24] N. Jorapur, V. S. Palaparthy, S. Sarik, J. John, M. S. Baghini, and G. K. Ananthasuresh, "A low-power, low-cost soil-moisture sensor using dual-probe heat-pulse technique," *Sens. Actuators A, Phys.*, vol. 233, pp. 108–117, Sep. 2015.
[25] *229-L—Heat Dissipation Matric Potential Sensor*. Accessed: Jul. 27, 2020. [Online]. Available: httpshttps://www.campbellsci.com/229-l
[26] J. Kodikara, P. Rajeev, D. Chan, and C. Gallage, "Soil moisture monitoring at the field scale using neutron probe," *Can. Geotech. J.*, vol. 51, no. 3, pp. 332–345, Mar. 2014.
[27] B. Kashyap, C. K. Sestok, A. G. Dabak, S. Ramaswamy, and R. Kumar, "Ultra-precision liquid level sensing using impedance spectroscopy and data analytics," *IEEE Sensors J.*, vol. 19, no. 20, pp. 9468–9478, Oct. 2019.
[28] G. C. Topp, J. L. Davis, and A. P. Annan, "Electromagnetic determination of soil water content: Measurements in coaxial transmission lines," *Water Resour. Res.*, vol. 16, no. 3, pp. 574–582, Jun. 1980.
[29] K. Noborio, "Measurement of soil water content and electrical conductivity by time domain reflectometry: A review," *Comput. Electron. Agricult.*, vol. 31, no. 3, pp. 213–237, May 2001.
[30] H. Quinones, P. Ruelle, and I. Nemeth, "Comparison of three calibration procedures for TDR soil moisture sensors," *Irrigation Drainage*, vol. 52, no. 3, pp. 203–217, 2003.
[31] W. Skierucha, "Temperature dependence of time domain reflectometry-measured soil dielectric permittivity," *J. Plant Nutrition Soil Sci.*, vol. 172, no. 2, pp. 186–193, Apr. 2009.
[32] M. Dobson, F. Ulaby, M. Hallikainen, and M. El-Rayes, "Microwave dielectric behavior of wet soil—Part II: Dielectric mixing models," *IEEE Trans. Geosci. Remote Sens.*, vol. GE-23, no. 1, pp. 35–46, Jan. 1985.
[33] *FieldScout TDR 350 Soil Moisture Meter With Case | Spectrum Technologies*. Accessed: Oct. 29, 2020. [Online]. Available: https://www.specmeters.com/soil-and-water/soil-moisture/fieldscout-tdr-meters/fieldscout-tdr-350-soil-moisture-meter-with-case/
[34] P. P. Bobrov, A. V. Repin, and O. V. Rodionova, "Wideband frequency domain method of soil dielectric property measurements," *IEEE Trans. Geosci. Remote Sens.*, vol. 53, no. 5, pp. 2366–2372, May 2015.
[35] J. González-Teruel, R. Torres-Sánchez, P. Blaya-Ros, A. Toledo-Moreo, M. Jiménez-Buendía, and F. Soto-Valles, "Design and calibration of a low-cost SDI-12 soil moisture sensor," *Sensors*, vol. 19, no. 3, p. 491, Jan. 2019.
[36] G. Pandey, R. J. Weber, and R. Kumar, "Agricultural cyber-physical system: *In-situ* soil moisture and salinity estimation by dielectric mixing," *IEEE Access*, vol. 6, pp. 43179–43191, 2018.
[37] G. Pandey, R. Kumar, and R. J. Weber, "Low RF-band impedance spectroscopy based sensor for *in-situ*, wireless soil sensing," U.S. Patent 10 073 074, Sep. 11, 2018.
[38] C. Rusu, A. Krozer, C. Johansson, F. Ahrentorp, T. Pettersson, C. Jonasson, J. Rösevall, D. Ilver, M. Terzaghi, D. Chiatante, and A. Montagnoli, "Miniaturized wireless water content and conductivity soil sensor system," *Comput. Electron. Agricult.*, vol. 167, Dec. 2019, Art. no. 105076.
[39] *Decagon MPS6 Meter Group TEROS 21 Water Potential Sensor | ICT International*. Accessed: Oct. 29, 2020. [Online]. Available: https://www.ictinternational.com/products/mps-6/teros-21-water-potential-sensor/
[40] T. Schmugge, "Remote sensing of surface soil moisture," *J. Appl. Meteorol.*, vol. 17, no. 10, pp. 1549–1557, 1978.
[41] B. P. Mohanty, M. H. Cosh, V. Lakshmi, and C. Montzka, "Soil moisture remote sensing: State-of-the-science," *Vadose Zone J.*, vol. 16, no. 1, pp. 1–9, 2017.
[42] *NASA Launches Groundbreaking Soil Moisture Mapping Satellite*. Accessed: Aug. 21, 2020. [Online]. Available: http://www.nasa.gov/press/2015/january/nasa-launches-groundbreaking-soil-moisture-mapping-satellite
[43] S. K. Chan *et al.*, "Assessment of the SMAP passive soil moisture product," *IEEE Trans. Geosci. Remote Sens.*, vol. 54, no. 8, pp. 4994–5007, Aug. 2016.
[44] M. S. Burgin, A. Colliander, E. G. Njoku, S. K. Chan, F. Cabot, Y. H. Kerr, R. Bindlish, T. J. Jackson, D. Entekhabi, and S. H. Yueh, "A comparative study of the SMAP passive soil moisture product with existing satellite-based soil moisture products," *IEEE Trans. Geosci. Remote Sens.*, vol. 55, no. 5, pp. 2959–2971, May 2017.

[45] E. Babaeian, M. Sadeghi, S. B. Jones, C. Montzka, H. Vereecken, and M. Tuller, "Ground, proximal, and satellite remote sensing of soil moisture," *Rev. Geophys.*, vol. 57, no. 2, pp. 530–616, Jun. 2019.

[46] D. Zhang and G. Zhou, "Estimation of soil moisture from optical and thermal remote sensing: A review," *Sensors*, vol. 16, no. 8, p. 1308, Aug. 2016.

[47] S. A. Bowers and S. J. Smith, "Spectrophotometric determination of soil water content," *Soil Sci. Soc. Amer. J.*, vol. 36, no. 6, pp. 978–980, Nov. 1972.

[48] C. J. Tomlinson, L. Chapman, J. E. Thornes, and C. Baker, "Remote sensing land surface temperature for meteorology and climatology: A review," *Meteorol. Appl.*, vol. 18, no. 3, pp. 296–306, Sep. 2011.

[49] M. Sadeghi, E. Babaeian, M. Tuller, and S. B. Jones, "The optical trapezoid model: A novel approach to remote sensing of soil moisture applied to sentinel-2 and Landsat-8 observations," *Remote Sens. Environ.*, vol. 198, pp. 52–68, Sep. 2017.

[50] Y.-A. Liou and S. Kar, "Evapotranspiration estimation with remote sensing and various surface energy balance algorithms—A review," *Energies*, vol. 7, no. 5, pp. 2821–2849, Apr. 2014.

[51] I. Sandholt, K. Rasmussen, and J. Andersen, "A simple interpretation of the surface temperature/vegetation index space for assessment of surface moisture status," *Remote Sens. Environ.*, vol. 79, nos. 2–3, pp. 213–224, Feb. 2002.

[52] L. Karthikeyan, M. Pan, N. Wanders, D. N. Kumar, and E. F. Wood, "Four decades of microwave satellite soil moisture observations: Part 1. A review of retrieval algorithms," *Adv. Water Resour.*, vol. 109, pp. 106–120, Nov. 2017.

[53] I. Ali, F. Greifeneder, J. Stamenkovic, M. Neumann, and C. Notarnicola, "Review of machine learning approaches for biomass and soil moisture retrievals from remote sensing data," *Remote Sens.*, vol. 7, no. 12, pp. 16398–16421, Dec. 2015.

[54] K. Wu, G. A. Rodriguez, M. Zajc, E. Jacquemin, M. Clément, A. De Coster, and S. Lambot, "A new drone-borne GPR for soil moisture mapping," *Remote Sens. Environ.*, vol. 235, Dec. 2019, Art. no. 111456.

[55] S. Lambot, E. C. Slob, I. van den Bosch, B. Stockbroeckx, and M. Vanclooster, "Modeling of ground-penetrating radar for accurate characterization of subsurface electric properties," *IEEE Trans. Geosci. Remote Sens.*, vol. 42, no. 11, pp. 2555–2568, Nov. 2004.

[56] L. Zhang, H. Zhang, Y. Niu, and W. Han, "Mapping maize water stress based on UAV multispectral remote sensing," *Remote Sens.*, vol. 11, no. 6, p. 605, Mar. 2019.

[57] Utah State University. *Aggieair*. Accessed: Oct. 29, 2020. [Online]. Available: https://uwrl.usu.edu/aggieair/index.

[58] L. Hassan-Esfahani, A. Torres-Rua, A. Jensen, and M. McKee, "Assessment of surface soil moisture using high-resolution multi-spectral imagery and artificial neural networks," *Remote Sens.*, vol. 7, no. 3, pp. 2627–2646, Mar. 2015.

[59] N. J. Stehr, "Drones: The newest technology for precision agriculture," *Natural Sci. Edu.*, vol. 44, no. 1, pp. 89–91, Dec. 2015.

[60] *Unmanned Aircraft Systems (UAS)*. Accessed: Jul. 19, 2020. [Online]. Available: https://www.faa.gov/uas/

[61] J. A. Doolittle and E. C. Brevik, "The use of electromagnetic induction techniques in soils studies," *Geoderma*, vol. 223–225, pp. 33–45, Jul. 2014.

[62] A. Salam, M. C. Vuran, and S. Irmak, "Di-sense: *In situ* real-time permittivity estimation and soil moisture sensing using wireless underground communications," *Comput. Netw.*, vol. 151, pp. 31–41, Mar. 2019.

[63] A. M. Peterson, W. D. Helgason, and A. M. Ireson, "Estimating field-scale root zone soil moisture using the cosmic-ray neutron probe," *Hydrol. Earth Syst. Sci.*, vol. 20, no. 4, pp. 1373–1385, Apr. 2016.

[64] *PC-Progress—Hydrus-1D Description*. Accessed: Oct. 27, 2020. [Online]. Available: https://www.pc-progress.com/en/Default.aspx?h1d-description

[65] L. Lv, T. E. Franz, D. A. Robinson, and S. B. Jones, "Measured and modeled soil moisture compared with cosmic-ray neutron probe estimates in a mixed forest," *Vadose Zone J.*, vol. 13, no. 12, Dec. 2014, Art. no. vzj2014.06.0077.

[66] M. Zreda, W. J. Shuttleworth, X. Zeng, C. Zweck, D. Desilets, T. Franz, and R. Rosolem, "COSMOS: The COsmic-ray soil moisture observing system," *Hydrol. Earth Syst. Sci.*, vol. 16, no. 11, pp. 4079–4099, Nov. 2012.

[67] H. H. Nguyen, J. Jeong, and M. Choi, "Extension of cosmic-ray neutron probe measurement depth for improving field scale root-zone soil moisture estimation by coupling with representative *in-situ* sensors," *J. Hydrol.*, vol. 571, pp. 679–696, Apr. 2019.

[68] N. Rodriguez-Alvarez, X. Bosch-Lluis, A. Camps, A. Aguasca, M. Vall-llossera, E. Valencia, I. Ramos-Perez, and H. Park, "Review of crop growth and soil moisture monitoring from a ground-based instrument implementing the interference pattern GNSS-R technique," *Radio Sci.*, vol. 46, no. 6, pp. 1–11, Dec. 2011.

[69] C. C. Chew, E. E. Small, K. M. Larson, and V. U. Zavorotny, "Effects of near-surface soil moisture on GPS SNR data: Development of a retrieval algorithm for soil moisture," *IEEE Trans. Geosci. Remote Sens.*, vol. 52, no. 1, pp. 537–543, Jan. 2014.

[70] K. M. Larson, J. J. Braun, E. E. Small, V. U. Zavorotny, E. D. Gutmann, and A. L. Bilich, "GPS multipath and its relation to near-surface soil moisture content," *IEEE J. Sel. Topics Appl. Earth Observ. Remote Sens.*, vol. 3, no. 1, pp. 91–99, Mar. 2010.

[71] S. Vey, A. Güntner, J. Wickert, T. Blume, and M. Ramatschi, "Long-term soil moisture dynamics derived from GNSS interferometric reflectometry: A case study for Sutherland, South Africa," *GPS Solutions*, vol. 20, no. 4, pp. 641–654, Oct. 2016.

[72] Inc Soil Scout. *Wireless Soil Moisture Sensors*. Accessed: Oct. 30, 2020. [Online]. Available: http://soilscout.com/solution/elements/

[73] F. R. Troeh and L. M. Thompson, *Soils and Soil Fertility*, 6th ed. Hoboken, NJ, USA: Wiley, 2005.

[74] *Soil and Water Testing*. Accessed: Jul. 24, 2020. [Online]. Available: https://www.sedgwick.k-state.edu/products-test/soiltests.html

[75] *Sampling Instructions for Routine Soil Analysis*. Accessed: Jul. 24, 2020. [Online]. Available: https://ag.umass.edu/soil-plant-nutrient-testing-laboratory/fact-sheets/sampling-instructions-for-routine-soil-analysis

[76] J. R. Brown, "Recommended chemical soil tests procedures for the North Central region," Rev. ed. North Central Regional Publ. 221, 1998.

[77] J. R. Okalebo, K. W. Gathua, and P. L. Woomer, *Laboratory Methods of Soil and Plant Analysis: A Working Manual*. Nairobi, Kenya: TSBF, 1993.

[78] C. Dimkpa, P. Bindraban, J. E. McLean, L. Gatere, U. Singh, and D. Hellums, "Methods for rapid testing of plant and soil nutrients," in *Sustainable Agriculture Reviews*. Cham, Switzerland: Springer, 2017, pp. 1–43.

[79] N. Moonrungsee, S. Pencharee, and J. Jakmunee, "Colorimetric analyzer based on mobile phone camera for determination of available phosphorus in soil," *Talanta*, vol. 136, pp. 204–209, May 2015.

[80] *Model STH-5—Soil Testing Outfit*. Accessed: Jul. 24, 2020. [Online]. Available: https://lamotte.com/products/soil/agricultural-soil-testing-kits/model-sth-5-soil-testing-outfit

[81] *About ICP Analysis*. Accessed: Jul. 25, 2020. [Online]. Available: https://soiltest.vt.edu/content/soiltest_vt_edu/en/Files/labinfo.html

[82] A. D. Karathanasis and B. F. Hajek, *Elemental Analysis by X-Ray Fluorescence Spectroscopy*. Hoboken, NJ, USA: Wiley, 2018, ch. 7, pp. 161–223.

[83] D. T. Jackson and P. N. Nelson, "Preparation and properties of some ion selective membranes: A review," *J. Mol. Struct.*, vol. 1182, pp. 241–259, Apr. 2019.

[84] A. Craggs, G. J. Moody, and J. D. R. Thomas, "PVC matrix membrane ion-selective electrodes. Construction and laboratory experiments," *J. Chem. Educ.*, vol. 51, no. 8, p. 541, Aug. 1974.

[85] S. Birrell and J. W. Hummel, "Membrane selection and ISFET configuration evaluation for soil nitrate sensing," *Trans. Amer. Soc. Agricult. Eng.*, vol. 43, pp. 197–206, Mar. 2000.

[86] M. Fibbioli, W. E. Morf, M. Badertscher, N. F. de Rooij, and E. Pretsch, "Potential drifts of solid-contacted ion-selective electrodes due to zero-current ion fluxes through the sensor membrane," *Electroanalysis*, vol. 12, no. 16, pp. 1286–1292, Nov. 2000.

[87] S. Komaba, T. Akatsuka, K. Ohura, C. Suzuki, N. Yabuuchi, S. Kanazawa, K. Tsuchiya, and T. Hasegawa, "All-solid-state ion-selective electrodes with redox-active lithium, sodium, and potassium insertion materials as the inner solid-contact layer," *Analyst*, vol. 142, no. 20, pp. 3857–3866, 2017.

[88] J. Bobacka, "Conducting polymer-based solid-state ion-selective electrodes," *Electroanalysis*, vol. 18, no. 1, pp. 7–18, Jan. 2006.

[89] M. Chen, M. Zhang, X. Wang, Q. Yang, M. Wang, G. Liu, and L. Yao, "An all-solid-state nitrate ion-selective electrode with nanohybrids composite films for *in-situ* soil nutrient monitoring," *Sensors*, vol. 20, no. 8, p. 2270, Apr. 2020.

[90] H. Jiang, W. Yu, J. F. Waimin, N. Glassmaker, N. Raghunathan, X. Jiang, B. Ziaie, and R. Rahimi, "Inkjet-printed solid-state potentiometric nitrate ion selective electrodes for agricultural application," in *Proc. IEEE SENSORS*, Oct. 2019, pp. 1–4.
[91] M. A. Ali, X. Wang, Y. Chen, Y. Jiao, N. K. Mahal, S. Moru, M. J. Castellano, J. C. Schnable, P. S. Schnable, and L. Dong, "Continuous monitoring of soil nitrate using a miniature sensor with poly(3-octyl-thiophene) and molybdenum disulfide nanocomposite," *ACS Appl. Mater. Interfaces*, vol. 11, no. 32, pp. 29195–29206, Aug. 2019.
[92] J. Choosang, A. Numnuam, P. Thavarungkul, P. Kanatharana, T. Radu, S. Ullah, and A. Radu, "Simultaneous detection of ammonium and nitrate in environmental samples using on ion-selective electrode and comparison with portable colorimetric assays," *Sensors*, vol. 18, no. 10, p. 3555, Oct. 2018.
[93] M. Pięk, R. Piech, and B. Paczosa-Bator, "TTF-TCNQ solid contact layer in all-solid-state ion-selective electrodes for potassium or nitrate determination," *J. Electrochem. Soc.*, vol. 165, no. 2, pp. B60–B65, 2018.
[94] N. T. Garland, E. S. McLamore, N. D. Cavallaro, D. Mendivelso-Perez, E. A. Smith, D. Jing, and J. C. Claussen, "Flexible laser-induced graphene for nitrogen sensing in soil," *ACS Appl. Mater. Interfaces*, vol. 10, no. 45, pp. 39124–39133, Nov. 2018.
[95] C. Wardak, "Solid contact nitrate ion-selective electrode based on ionic liquid with stable and reproducible potential," *Electroanalysis*, vol. 26, no. 4, pp. 864–872, Apr. 2014.
[96] Mettler-TOLEDO International Inc. *Perfection Comb NO3 Lemo*. Accessed: Jul 3, 2020. [Online]. Available: https://www.mt.com/us/en/home/products/Laboratory_Analytics_Browse/pH-meter/sensor/ion-selective-electrode/perfectIONComb-NO3-Lemo.shop.html
[97] *Vernier Nitrate Ion-Selective Electrode*. Accessed: Jul. 3, 2020. [Online]. Available: https://www.vernier.com/product/nitrate-ion-selective-electrode/
[98] T. Hachiya and H. Sakakibara, "Interactions between nitrate and ammonium in their uptake, allocation, assimilation, and signaling in plants," *J. Experim. Botany*, vol. 68, no. 10, pp. 2501–2512, 12 2016.
[99] H. Kim, K. A. Sudduth, and J. W. Hummel, "Soil macronutrient sensing for precision agriculture," *J. Environ. Monitoring*, vol. 11, no. 10, pp. 1810–1824, 2009.
[100] H. J. Nielsen and E. H. Hansen, "New nitrate ion-selective electrodes based on quaternary ammonium compounds in nonporous polymer membranes," *Anal. Chim. Acta*, vol. 85, no. 1, pp. 1–16, Aug. 1976.
[101] T. M. Mubita, J. E. Dykstra, P. M. Biesheuvel, A. van der Wal, and S. Porada, "Selective adsorption of nitrate over chloride in microporous carbons," *Water Res.*, vol. 164, Nov. 2019, Art. no. 114885.
[102] M. B. Arvas, O. Gorduk, M. Gencten, and Y. Sahin, "Preparation of a novel electrochemical sensor for phosphate detection based on a molybdenum blue modified poly(vinyl chloride) coated pencil graphite electrode," *Anal. Methods*, vol. 11, no. 30, pp. 3874–3881, 2019.
[103] S. Sedaghat, S. Jeong, A. Zareei, S. Peana, N. Glassmaker, and R. Rahimi, "Development of a nickel oxide/oxyhydroxide-modified printed carbon electrode as an all solid-state sensor for potentiometric phosphate detection," *New J. Chem.*, vol. 43, no. 47, pp. 18619–18628, 2019.
[104] K. S. Bhat, U. T. Nakate, J.-Y. Yoo, Y. Wang, T. Mahmoudi, and Y.-B. Hahn, "Nozzle-jet-printed silver/graphene composite-based field-effect transistor sensor for phosphate ion detection," *ACS Omega*, vol. 4, no. 5, pp. 8373–8380, May 2019.
[105] V. O. Ebuele, D. G. Congrave, C. D. Gwenin, and V. Fitzsimmons-Thoss, "Development of a cobalt electrode for the determination of phosphate in soil extracts and comparison with standard methods," *Anal. Lett.*, vol. 51, no. 6, pp. 834–848, Apr. 2018.
[106] K. Xu, Y. Kitazumi, K. Kano, and O. Shirai, "Phosphate ion sensor using a cobalt phosphate coated cobalt electrode," *Electrochim. Acta*, vol. 282, pp. 242–246, Aug. 2018.
[107] L. Barhoumi, A. Baraket, N. M. Nooredeen, M. B. Ali, M. N. Abbas, J. Bausells, and A. Errachid, "Silicon nitride capacitive chemical sensor for phosphate ion detection based on copper phthalocyanine–acrylate-polymer," *Electroanalysis*, vol. 29, no. 6, pp. 1586–1595, Jun. 2017.
[108] S. Cinti, D. Talarico, G. Palleschi, D. Moscone, and F. Arduini, "Novel reagentless paper-based screen-printed electrochemical sensor to detect phosphate," *Anal. Chim. Acta*, vol. 919, pp. 78–84, May 2016.
[109] M. N. Abbas, A. L. A. Radwan, N. M. Nooredeen, and M. A. A. El-Ghaffar, "Selective phosphate sensing using copper monoamino-phthalocyanine functionalized acrylate polymer-based solid-state electrode for FIA of environmental waters," *J. Solid State Electrochem.*, vol. 20, no. 6, pp. 1599–1612, Jun. 2016.
[110] P. Kumar, D.-M. Kim, M. H. Hyun, M.-S. Won, and Y.-B. Shim, "An all solid state potentiometric sensor for monohydrogen phosphate ions," *Electroanalysis*, vol. 25, no. 8, pp. 1864–1870, Aug. 2013.
[111] *Understanding Soil Tests for Pastures—Agriculture*. Accessed: Aug. 5, 2020. [Online]. Available: https://agriculture.vic.gov.au/farm-management/soil/understanding-soil-tests-for-pastures
[112] D. Liu, W.-C. Chen, R.-H. Yang, G.-L. Shen, and R.-Q. Yu, "Polymeric membrane phosphate sensitive electrode based on binuclear organotin compound," *Anal. Chim. Acta*, vol. 338, no. 3, pp. 209–214, Feb. 1997.
[113] J. H. Yoon, H. J. Park, S. H. Park, K. G. Lee, and B. G. Choi, "Electrochemical characterization of reduced graphene oxide as an ion-to-electron transducer and application of screen-printed all-solid-state potassium ion sensors," *Carbon Lett.*, vol. 30, pp. 73–80, 2020.
[114] I. Fakih, A. Centeno, A. Zurutuza, B. Ghaddab, M. Siaj, and T. Szkopek, "High resolution potassium sensing with large-area graphene field-effect transistors," *Sens. Actuators B, Chem.*, vol. 291, pp. 89–95, Jul. 2019.
[115] R. Rosenberg, M. S. Bono, S. Braganza, C. Vaishnav, R. Karnik, and A. J. Hart, "In-field determination of soil ion content using a hand-held device and screen-printed solid-state ion-selective electrodes," *PLoS ONE*, vol. 13, no. 9, pp. 1–20, Sep. 2018.
[116] K. Yu, N. He, N. Kumar, N. Wang, J. Bobacka, and A. Ivaska, "Electrosynthesized polypyrrole/zeolite composites as solid contact in potassium ion-selective electrode," *Electrochim. Acta*, vol. 228, pp. 66–75, Feb. 2017.
[117] B. Paczosa-Bator, "Ion-selective electrodes with superhydrophobic polymer/carbon nanocomposites as solid contact," *Carbon*, vol. 95, pp. 879–887, Dec. 2015.
[118] F. Li, J. Ye, M. Zhou, S. Gan, Q. Zhang, D. Han, and L. Niu, "All-solid-state potassium-selective electrode using graphene as the solid contact," *Analyst*, vol. 137, no. 3, pp. 618–623, 2012.
[119] *Potassium Ion-Selective Electrode*. Accessed: Aug. 5, 2020. [Online]. Available: https://www.vernier.com/product/potassium-ion-selective-electrode/
[120] *Perfection Comb K Lemo*. Accessed: Aug. 5, 2020. [Online]. Available: https://www.mt.com/us/en/home/products/Laboratory_Analytics_Browse/pH-meter/sensor/ion-selective-electrode/perfectION-Comb-K-Lemo.html
[121] W. Gao, S. Emaminejad, H. Y. Y. Nyein, S. Challa, K. Chen, A. Peck, H. M. Fahad, H. Ota, H. Shiraki, D. Kiriya, D.-H. Lien, G. A. Brooks, R. W. Davis, and A. Javey, "Fully integrated wearable sensor arrays for multiplexed *in situ* perspiration analysis," *Nature*, vol. 529, no. 7587, pp. 509–514, Jan. 2016.
[122] *Potassium for Crop Production*. Accessed: Aug. 4, 2020. [Online]. Available: https://extension.umn.edu/phosphorus-and-potassium/potassium-crop-production
[123] H.-J. Kim, W.-K. Kim, M.-Y. Roh, C.-I. Kang, J.-M. Park, and K. A. Sudduth, "Automated sensing of hydroponic macronutrients using a computer-controlled system with an array of ion-selective electrodes," *Comput. Electron. Agricult.*, vol. 93, pp. 46–54, Apr. 2013.
[124] M. Novell, M. Parrilla, G. A. Crespo, F. X. Rius, and F. J. Andrade, "Paper-based ion-selective potentiometric sensors," *Anal. Chem.*, vol. 84, no. 11, pp. 4695–4702, Jun. 2012.
[125] W.-J. Lan, X. U. Zou, M. M. Hamedi, J. Hu, C. Parolo, E. J. Maxwell, P. Bühlmann, and G. M. Whitesides, "Paper-based potentiometric ion sensing," *Anal. Chem.*, vol. 86, no. 19, pp. 9548–9553, Oct. 2014.
[126] R. S. Patkar, M. Ashwin, and V. R. Rao, "Piezoresistive microcantilever based lab-on-a-chip system for detection of macronutrients in the soil," *Solid-State Electron.*, vol. 138, pp. 94–100, Dec. 2017.
[127] M. A. Ali, H. Jiang, N. K. Mahal, R. J. Weber, R. Kumar, M. J. Castellano, and L. Dong, "Microfluidic impedimetric sensor for soil nitrate detection using graphene oxide and conductive nanofibers enabled sensing interface," *Sens. Actuators B, Chem.*, vol. 239, pp. 1289–1299, Feb. 2017.
[128] T. Minami, Y. Sasaki, T. Minamiki, S.-I. Wakida, R. Kurita, O. Niwa, and S. Tokito, "Selective nitrate detection by an enzymatic sensor based on an extended-gate type organic field-effect transistor," *Biosensors Bioelectron.*, vol. 81, pp. 87–91, Jul. 2016.
[129] J. Massah and K. A. Vakilian, "An intelligent portable biosensor for fast and accurate nitrate determination using cyclic voltammetry," *Biosyst. Eng.*, vol. 177, pp. 49–58, Jan. 2019.
[130] K. A. Vakilian and J. Massah, "A portable nitrate biosensing device using electrochemistry and spectroscopy," *IEEE Sensors J.*, vol. 18, no. 8, pp. 3080–3089, Apr. 2018.
[131] F. Can, S. Korkut Ozoner, P. Ergenekon, and E. Erhan, "Amperometric nitrate biosensor based on carbon nanotube/polypyrrole/nitrate reductase biofilm electrode," *Mater. Sci. Eng., C*, vol. 32, no. 1, pp. 18–23, Jan. 2012.

[132] M. E. E. Alahi, S. C. Mukhopadhyay, and L. Burkitt, "Imprinted polymer coated impedimetric nitrate sensor for real-time water quality monitoring," *Sens. Actuators B, Chem.*, vol. 259, pp. 753–761, Apr. 2018.
[133] E. Bomar, G. Owens, and G. Murray, "Nitrate ion selective electrode based on ion imprinted poly(N-methylpyrrole)," *Chemosensors*, vol. 5, no. 1, p. 2, Jan. 2017.
[134] H. Bagheri, A. Hajian, M. Rezaei, and A. Shirzadmehr, "Composite of Cu metal nanoparticles-multiwall carbon nanotubes-reduced graphene oxide as a novel and high performance platform of the electrochemical sensor for simultaneous determination of nitrite and nitrate," *J. Hazardous Mater.*, vol. 324, pp. 762–772, Feb. 2017.
[135] J. Liang, Y. Zheng, and Z. Liu, "Nanowire-based cu electrode as electrochemical sensor for detection of nitrate in water," *Sens. Actuators B, Chem.*, vol. 232, pp. 336–344, Sep. 2016.
[136] L. Gilbert, A. T. A. Jenkins, S. Browning, and J. P. Hart, "Development of an amperometric, screen-printed, single-enzyme phosphate ion biosensor and its application to the analysis of biomedical and environmental samples," *Sens. Actuators B, Chem.*, vol. 160, no. 1, pp. 1322–1327, Dec. 2011.
[137] R. Ahmad, M.-S. Ahn, and Y.-B. Hahn, "ZnO nanorods array based field-effect transistor biosensor for phosphate detection," *J. Colloid Interface Sci.*, vol. 498, pp. 292–297, Jul. 2017.
[138] G. Kopiec, K. Starzec, J. Kochana, T. P. Kinnunen-Skidmore, W. Schuhmann, W. H. Campbell, A. Ruff, and N. Plumeré, "Bioelectrocatalytic and electrochemical cascade for phosphate sensing with up to 6 electrons per analyte molecule," *Biosensors Bioelectron.*, vol. 117, pp. 501–507, Oct. 2018.
[139] C. Storer, Z. Coldrick, D. Tate, J. Donoghue, and B. Grieve, "Towards phosphate detection in hydroponics using molecularly imprinted polymer sensors," *Sensors*, vol. 18, no. 2, p. 531, Feb. 2018.
[140] V. Borse, P. Jain, M. Sadawana, and R. Srivastava, "'Turn-on' fluorescence assay for inorganic phosphate sensing," *Sens. Actuators B, Chem.*, vol. 225, pp. 340–347, Mar. 2016.
[141] M. Sarwar, J. Leichner, G. M. Naja, and C.-Z. Li, "Smart-phone, paper-based fluorescent sensor for ultra-low inorganic phosphate detection in environmental samples," *Microsyst. Nanoeng.*, vol. 5, no. 1, p. 56, Dec. 2019.
[142] M. Naderi, M. Hosseini, and M. R. Ganjali, "Naked-eye detection of potassium ions in a novel gold nanoparticle aggregation-based aptasensor," *Spectrochimica Acta A, Mol. Biomolecular Spectrosc.*, vol. 195, pp. 75–83, Apr. 2018.
[143] X. Liu, C. Ye, X. Li, N. Cui, T. Wu, S. Du, Q. Wei, L. Fu, J. Yin, and C.-T. Lin, "Highly sensitive and selective potassium ion detection based on graphene Hall effect biosensors," *Materials*, vol. 11, no. 3, p. 399, Mar. 2018.
[144] J. Ning, X. Lin, F. Su, A. Sun, H. Liu, J. Luo, L. Wang, and Y. Tian, "Development of a molecular K+ probe for colorimetric/fluorescent/photoacoustic detection of K+," *Anal. Bioanal. Chem.*, vol. 412, no. 25, pp. 6947–6957, Oct. 2020.
[145] N. Rogovska, D. A. Laird, C.-P. Chiou, and L. J. Bond, "Development of field mobile soil nitrate sensor technology to facilitate precision fertilizer management," *Precis. Agricult.*, vol. 20, no. 1, pp. 40–55, Feb. 2019.
[146] T. R. Tavares, L. C. Nunes, E. E. N. Alves, E. D. Almeida, L. F. Maldaner, F. J. Krug, H. W. P. D. Carvalho, and J. P. Molin, "Simplifying sample preparation for soil fertility analysis by X-ray fluorescence spectrometry," *Sensors*, vol. 19, no. 23, p. 5066, Nov. 2019.
[147] X. An, M. Li, L. Zheng, Y. Liu, and H. Sun, "A portable soil nitrogen detector based on NIRS," *Precis. Agricult.*, vol. 15, no. 1, pp. 3–16, Feb. 2014.
[148] J. W. Jorgenson and K. D. Lukacs, "Zone electrophoresis in open-tubular glass capillaries," *Anal. Chem.*, vol. 53, no. 8, pp. 1298–1302, Jul. 1981.
[149] *7100 CE System | Agilent*. Accessed: Jul. 13, 2020. [Online]. Available: https://www.agilent.com/en/product/capillary-electrophoresis-ce-ms/ce-ce-ms-systems/7100-ce-system
[150] *LabChip GX Touch Nucleic Acid Analyzer*. Accessed: Jul. 13, 2020. [Online]. Available: https://perkinelmer-appliedgenomics.com/home/products/nucleic-acid-analysis-protein-characterization/dna-rna-analysis-microfluidics-technology/labchip-gx-touch-nucleic-acid-analyzer/
[151] Z. Xu, X. Wang, R. J. Weber, R. Kumar, and L. Dong, "Nutrient sensing using chip scale electrophoresis and *in situ* soil solution extraction," *IEEE Sensors J.*, vol. 17, no. 14, pp. 4330–4339, Jul. 2017.
[152] M. Smolka, D. Puchberger-Enengl, M. Bipoun, A. Klasa, M. Kiczkajlo, W. Śmiechowski, P. Sowiński, C. Krutzler, F. Keplinger, and M. J. Vellekoop, "A mobile lab-on-a-chip device for on-site soil nutrient analysis," *Precis. Agricult.*, vol. 18, no. 2, pp. 152–168, Apr. 2017.
[153] C. Merusi, C. Corradini, A. Cavazza, C. Borromei, and P. Salvadeo, "Determination of nitrates, nitrites and oxalates in food products by capillary electrophoresis with pH-dependent electroosmotic flow reversal," *Food Chem.*, vol. 120, no. 2, pp. 615–620, May 2010.
[154] B. Westergaard and H. C. B. Hansen, "Determination of anions in soil solutions by capillary zone electrophoresis," *Analyst*, vol. 123, no. 4, pp. 721–724, 1998.
[155] K. Fukushi, S. Takeda, K. Chayama, and S.-I. Wakida, "Application of capillary electrophoresis to the analysis of inorganic ions in environmental samples," *J. Chromatogr. A*, vol. 834, nos. 1–2, pp. 349–362, Feb. 1999.
[156] Z. Xu, L. Dong, and R. Kumar, "Electrophoretic soil nutrient sensor for agriculture," U.S. Patent 10 564 122, Feb. 18, 2020.
[157] *Agriculture IoT Market—Global Opportunity Analysis and Industry Forecast (2019–2027)*. Accessed: Aug. 13, 2020. [Online]. Available: https://www.meticulousresearch.com/product/agriculture-iot-market-5080/
[158] H. Sahota, R. Kumar, and A. Kamal, "A wireless sensor network for precision agriculture and its performance," *Wireless Commun. Mobile Comput.*, vol. 11, no. 12, pp. 1628–1645, Dec. 2011.
[159] H. Sahota and R. Kumar, "Maximum-likelihood sensor node localization using received signal strength in multimedia with multipath characteristics," *IEEE Syst. J.*, vol. 12, no. 1, pp. 506–515, Mar. 2018.
[160] H. Sahota and R. Kumar, "Network based sensor localization in multimedia application of precision agriculture part 2: Time of arrival," in *Proc. 11th IEEE Int. Conf. Netw., Sens. Control*, Apr. 2014, pp. 203–208.

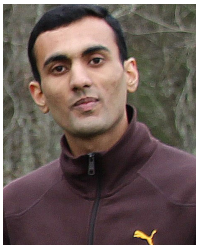

BHUWAN KASHYAP (Member, IEEE) received the B.Tech. degree in electronics and communication engineering from the Indian Institute of Technology Roorkee, India, in 2014. He is currently pursuing the Ph.D. degree in electrical engineering with Iowa State University, Ames, IA, USA. His current research interests include designing sensing technologies for sustainable agriculture, microwave engineering, micro-electro-mechanical systems, digital circuit design, lab-on-a-chip-based systems, and clean energy harvesting devices.

RATNESH KUMAR (Fellow, IEEE) received the B.Tech. degree in electrical engineering from IIT Kanpur, India, in 1987, and the M.S. and Ph.D. degrees in electrical and computer engineering from The University of Texas at Austin, in 1989 and 1991, respectively. He is currently a Harpole Professor with Iowa State University, Electrical and Computer Engineering, where he directs the ESSeNCE (Embedded Software, Sensors, Networks, Cyberphysical, and Energy) Lab. Previously, he held faulty position at the University of Kentucky, and various visiting positions with the University of Maryland (College Park), the Applied Research Laboratory at the Pennsylvania State University (State College), the NASA Ames, the Idaho National Laboratory, the United Technologies Research Center, and the Air Force Research Laboratory. He was a recipient of the Gold Medals for the Best EE Undergrad, the Best EE Project, and the Best All Rounder from IIT Kanpur, the Best Dissertation Award from UT Austin, the Best Paper Award from the IEEE Transactions on Automation Science and Engineering, and Keynote Speaker and paper awards recipient from multiple conferences. He is or has been an editor of several journals (including of IEEE, SIAM, ACM, Springer, IET, MDPI), was a Distinguished Lecturer of the IEEE Control Systems Society, was a recipient of D. R. Boylan Eminent Faculty Award for Research from Iowa State University and also a Fellow of AAAS.